



PCCP

**Single Atom Alloy vs Phase Separated Alloy in Cu, Ag, and Au atoms with Ni(111) and Ni, Pd, and Pt atoms with Cu(111):
Theoretical Exploration**

Journal:	<i>Physical Chemistry Chemical Physics</i>
Manuscript ID	CP-ART-02-2022-000578.R1
Article Type:	Paper
Date Submitted by the Author:	29-Mar-2022
Complete List of Authors:	Yin, Junqing; Kyoto University, Element Strategy Initiative for Catalysts and Batteries Ehara, Masahiro; Institute for Molecular Science, Sakaki, Shigeyoshi; Kyoto University, Fukui Institute for Fundamental Chemistry

SCHOLARONE™
Manuscripts

**Single Atom Alloy vs Phase Separated Alloy in Cu, Ag, and Au
atoms with Ni(111) and Ni, Pd, and Pt atoms with Cu(111):
Theoretical Exploration**

Junqing Yin,[†] Masahiro Ehara,^{†, ‡} and Shigeyoshi Sakaki^{†*}

[†] Elements Strategy Initiative for Catalysts and Batteries (ESICB), Kyoto University, Goryo-Ohara 1-30, Nishikyo-ku, Kyoto 615-8245, Japan

[‡] Institute for Molecular Science (IMS), Okazaki 444-8585, Japan

ABSTRACT: Single-atom alloy (SAA) consisting of abundant metal host and precious metal guest is promising catalyst to reduce cost without loss of activity. DFT calculations of Ni- and Cu-based alloys $nX/M(111)$ ($X = \text{Cu, Ag, or Au}$ for $M = \text{Ni}$; $X = \text{Ni, Pd, or Pt}$ for $M = \text{Cu}$; $n = 1 \sim 4$) reveal that phase-separated alloy (PSA) is produced by Cu atoms with Ni(111) but SAA is produced by Au atoms with Ni(111) and Pd and Pt atoms with Cu(111). In the Ni(111)-based Ag alloy and Cu(111)-based Ni alloy, relative stabilities of SAA and PSA depend on coverages of Ag on Ni(111) and Ni on Cu(111). Interaction energy (E_{int}) between X_n cluster and M(111) host is larger than that between one X atom and M(111) host, because the X_n cluster forms more bonding interactions with the M(111) host than does one X atom. When going from one X atom to X_4 cluster, the E_{int} values of Au and Pt clusters respectively with Ni(111) and Cu(111) increase to a lesser extent than those of Cu and Ni clusters respectively with Ni(111) and Cu(111). Consequently, Au and Pt atoms tend to form SAA respectively with Ni(111) and Cu(111) hosts compared to Cu and Ni atoms. This trend in the E_{int} value is determined by valence orbital energies of the X atom and X_n cluster. Cu atoms in $n\text{Cu}/\text{Ni}(111)$ have slightly positive charge but Ag atoms in $n\text{Ag}/\text{Ni}(111)$, Au atoms in $n\text{Au}/\text{Ni}(111)$, and Ni, Pd, and Pt atoms in $nX/\text{Cu}(111)$ ($X = \text{Ni, Pd, or Pt}$) have negative charge. The negative charge increases in the order $\text{Ag} < \text{Au}$ in $nX/\text{Ni}(111)$ and $\text{Ni} < \text{Pd} < \text{Pt}$ in $nX/\text{Cu}(111)$. The Fermi level lowers in energy in the order $n\text{Cu}/\text{Ni}(111) \geq \text{Ni}(111) > n\text{Ag}/\text{Ni}(111) > n\text{Au}/\text{Ni}(111)$ and $\text{Cu}(111) \geq n\text{Ni}/\text{Cu}(111) > n\text{Pd}/\text{Cu}(111) > n\text{Pt}/\text{Cu}(111)$. The d valence band center lowers in energy in almost the same order. CO adsorption energy decreases in the order $\text{Ni}(111) \sim n\text{Cu}/\text{Ni}(111) > n\text{Ag}/\text{Ni}(111) \sim n\text{Au}/\text{Ni}(111)$ and $\text{Cu}(111) > n\text{Ni}/\text{Cu}(111) > n\text{Pd}/\text{Cu}(111) > n\text{Pt}/\text{Cu}(111)$. These properties are explained based on the electronic structures.

1. INTRODUCTION

Precious metals have been often used as catalysts.¹⁻³ However, the amount of precious metal(s) must be reduced to lower the cost of the catalyst and preserve the resources on the earth. Recently, single-atom alloys (SAAs) have been reported as an excellent catalyst, in which precious metal atoms are atomically dispersed on abundant base metal host.^{4,5} The SAA is one of promising catalysts to use minimum amount of precious metal(s) without loss of activity. Therefore, its further development is desirable. However, we do not have enough knowledge about the SAA. For instance, one of the serious problems is the lack of the general understanding about the combination of metal elements which forms SAA and the reason(s) why. Also, the knowledge of electronic structure and reactivity of SAA is indispensable for effective use of SAA, but the knowledge is insufficient.

Because nickel and copper are abundant metal elements on the earth, they are used as a host metal to construct SAAs.⁶⁻¹⁰ In this regard, such Ni-based alloys as Au-Ni, Ag-Ni, Cu-Ni, Pd-Ni, and Pt-Ni alloys and such Cu-based alloys as Ni-Cu, Pd-Cu, and Pt-Cu alloys have been applied to methane reforming,¹¹ methane activation,¹² propane dehydrogenation,¹³ CO₂ methanation,¹⁴ water-gas shift reaction,¹⁵ and NO reduction.^{16,17} Recently, Ni-based SAA of Au attracts great interest, because bimetallic Au-Ni alloy supported on silica (SiO₂) exhibits excellent catalytic activity for NO-CO reaction.¹⁸⁻²⁰ Scanning tunneling microscopy image showed that Au atoms were atomically dispersed on the Ni surface.²¹ In the Au-Ni alloy, two important features have been discussed.^{22,23} In one, Au and Ni are immiscible to each other due to a substantial size-mismatch. In the other, the Au-based alloy bearing Ni atoms dispersed on the Au surface is not stable thermodynamically but the Ni-based alloy bearing Au atoms dispersed on the Ni surface is stable. In other words, the Ni-based SAA of Au is stable but the Au-based SAA of Ni is not. However, the reason is unclear.

Besides the Au-Ni alloy, Cu and Ni can form a solid solution.²⁴ $\text{Ni}_{50}\text{Cu}_{50}/\text{Al}_2\text{O}_3$ catalyst was prepared by the impregnation method,²⁵ where $\text{M}^1/\text{M}_m^2\text{O}_n$ represents that M^1 metal atoms exist on M_m^2O_n surface hereinafter. This catalyst exhibited high catalytic activity and durability in three-way catalytic reaction under both oxidative and reductive conditions. The similar $\text{Ni}_{14}\text{Cu}_{11}/\text{SiO}_2$ catalyst exhibited high activity comparable to the industrial catalyst $\text{Cu}/\text{ZnO}/\text{Al}_2\text{O}_3$ in CO hydrogenation to methanol.²⁵ X-ray diffraction pattern of this catalyst showed the presences of both Cu phase and Ni-Cu alloy phase, indicating that a phase-separated alloy (PSA) was formed. The similar $\text{Ni}_{75}\text{Cu}_{25}/\text{Al}_2\text{O}_3$ catalyst was reported to form a PSA.²⁶ The presence of the Cu phase on the Ni surface was further supported by classical molecular dynamics simulations showing that the Cu migration and enrichment on the Ni surface occurred at a high temperature.²⁷ On the other hand, the Cu-based SAA of Ni was prepared by depositing slowly Ni atoms on the Cu(111) single crystal at a surface temperature of 433 K.²⁸ Similarly, $\text{Ni}_{0.01}\text{Cu}$ and $\text{Ni}_{0.001}\text{Cu}$ alloys were prepared by depositing Ni on Cu nanoparticle surface supported on SiO_2 . The $\text{Ni}_{0.001}\text{Cu}$ alloy exhibited good performance in non-oxidative dehydrogenation reaction of ethanol.^{29,30} X-ray absorption spectroscopy indicated that Ni atoms were observed exclusively as a single atom in $\text{Ni}_{0.001}\text{Cu}$ and that both isolated Ni atoms and small Ni nanoclusters were observed in $\text{Ni}_{0.01}\text{Cu}$. These experimentally observed results suggest that the SAA is as stable as the PSA in the Cu-based Ni alloy and that the SAA is formed when the Ni amount is small but the PSA is formed when the Ni amount is large.

The findings discussed above lead us to several important open questions: (i) What kind of metal element forms SAA with Ni and Cu hosts? (ii) Why does Au element form an SAA with the Ni host but does Cu element form a PSA with the Ni host despite that both belong to group XI in the periodic table? (iii) How much different are the electronic structures and reactivities of SAA and PSA from those of pure Ni and Cu bulk metals and why? Although

many experimental and theoretical studies have been carried out on segregation properties, catalytic activities, and catalytic reactions of the Ni- and Cu-based alloys,^{18–20,25,31–36} no theoretical answer has been presented to the aforementioned open questions.

In this theoretical work, relative stabilities of Ni-based SAA and PSA with Cu, Ag, and Au elements and Cu-based SAA and PSA with Ni, Pd, and Pt elements are investigated using spin-polarized DFT calculations, where Ni(111) and Cu(111) are employed as hosts. These alloys are named respectively $nX^1/\text{Ni}(111)$ ($X^1 = \text{Cu, Ag, and Au; } n = 1 \sim 4$) and $nX^2/\text{Cu}(111)$ ($X^2 = \text{Ni, Pd, and Pt}$), where the n is the number of the X atoms on $M(111)$. Our purposes here are to obtain clear answers to the open questions mentioned above, correct knowledge, and well understanding of the SAA and PSA on the basis of the electronic structure of alloy. Throughout this work, we intended to present new and fundamental findings of relative stabilities, electronic structures, and reactivities of Ni- and Cu-based SAA and PSA.

2. COMPUTATIONAL METHODS AND MODELS

2.1. Methods

Spin-polarized periodic DFT calculations were performed using the Vienna ab initio simulation package (VASP).^{37,38} The Perdew-Burke-Ernzerhof (PBE) functional³⁹ was used. The plane wave basis sets were employed with a kinetic-energy cut-off of 400 eV for representing valence electrons.^{40,41} The projector augmented wave pseudopotentials were employed for core electrons. Geometry optimization was performed with thresholds of 0.01 eV/Å for maximum force and 10^{-5} eV for energy change.⁴² The partial occupancies were determined with the first-order Methfessel-Paxton scheme, where the smearing width of 0.2 eV was employed.⁴³ The Brillouin zone was sampled within a Monkhorst-Pack k-point grid of $4 \times 4 \times 1$ for calculations of all the surface models.⁴⁴ Dispersion correction was not added because geometries of fcc-Ni and fcc-Cu optimized without dispersion correction agreed with

the experimental ones, as described below. Also, the dispersion correction influenced little the M–C and C–O distances in CO adsorption on M(111) surface (M = Ni, Cu) and the relative stabilities of alloys, as described in Tables S1 and S2 of Supporting Information (SI). Density of states (DOS) was calculated with the Gaussian smearing scheme (the smearing width = 0.1 eV) within a k-point grid of $5 \times 5 \times 1$. The Bader charges were calculated using the program developed by Henkelman group.⁴⁵ Frontier orbital energies of X atom and X_n cluster were calculated using the Gaussian 16 program⁴⁶ with the B3LYP⁴⁷⁻⁴⁹ and PBE³⁹ functionals, where basis sets by Stuttgart-Dresden group^{50,51} were used with the corresponding effective-core potentials.

2.2. Models

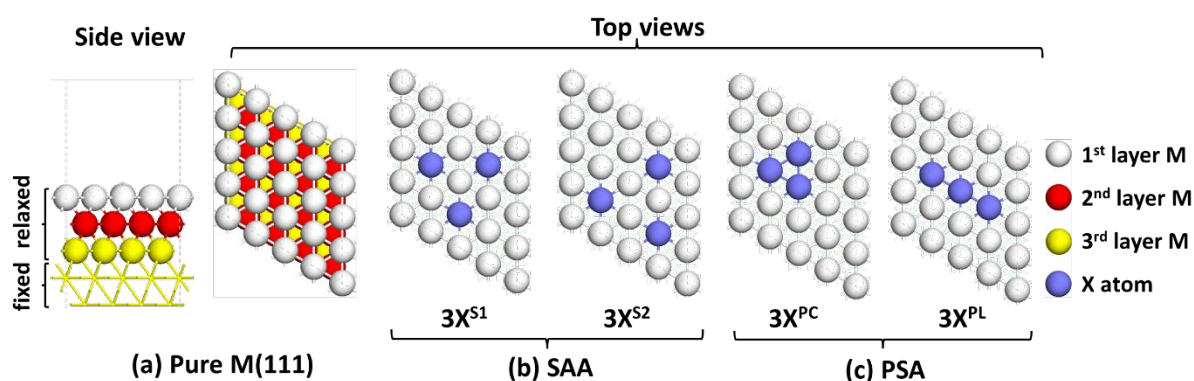
The lattice constants of bulk metals were optimized here to be 3.520 Å for fcc-Ni and 3.630 Å for fcc-Cu with a k-point grid of $9 \times 9 \times 9$. These optimized values agree with the experimental results, 3.52 Å for fcc-Ni and 3.62 Å for fcc-Cu.^{52,53} Using the optimized unit cells of fcc-Ni and fcc-Cu, we constructed Ni(111) and Cu(111) slab models adopting thickness of 5-layer atoms, supercell size of $p(4 \times 4)$, and vacuum layer of 15 Å between periodically repeated slabs, as shown in Scheme 1(a). Models of Ni-based alloys were constructed by replacing several Ni atoms of the surface with Cu, Ag, or Au atoms. Models of Cu-based alloys were constructed in a similar manner. The surface segregation energies reported by Nørskov and coworkers⁵⁴ indicate that Cu, Ag, and Au atoms prefer to stay on the Ni(111) surface and Pd and Pt atoms prefer to stay on the Cu(111) surface; indeed, our calculations clearly showed that in nCu/Ni(111), nAg/Ni(111), nAu/Ni(111), nPd/Cu(111) and nPt/Cu(111), Cu, Ag, Au, Pd, and Pt atoms exist on the surface rather than in the inside (Scheme S1 and Table S3 of the SI). However, the surface segregation energy indicates that Ni prefers to take an inside position of Cu(111).⁵⁴ We calculated Ni/Cu(111) bearing one Ni

atom at either the surface or the inside and found that the presence of Ni at the inside was slightly more stable than that at the surface, as shown in Table S3 of the SI. Although Ni atoms penetrate into Cu(111), the energy difference between Ni/Cu(111) bearing Ni atom on the surface and that bearing Ni atom at the inside is small. Also, several experimental observations suggested that Ni atoms existed on the surface of Cu nanoparticle in $\text{Ni}_{0.001}\text{Cu}$,²⁸⁻³⁰ as mentioned above, and the Ni atom was reported to take a surface position of Cu(111) in the presence of reactive adsorbate like CO.⁵⁵ These experimental and computational results suggest that the presence of atomically dispersed Ni atoms on the Cu(111) surface is not very unlikely. Therefore, we investigated the $n\text{Ni}/\text{Cu}(111)$ alloy bearing Ni atoms on the Cu(111) surface to make clear comparison of $n\text{Ni}/\text{Cu}(111)$ with $n\text{Pd}/\text{Cu}(111)$ and $n\text{Pt}/\text{Cu}(111)$.

The number (n) of X atoms placed at the M(111) surface was taken to be 1 ~ 4 in this work; the case of $n = 4$ corresponds to the X coverage of 25% of the surface monolayer. If the “ n ” is taken to be larger than 4, a perfect SAA structure cannot be constructed because of the constraint from the surface size of the slab model employed here. For instance, if “ n ” is larger than 5, two X atoms must be connected with each other on the surface. Because one of important purposes here is to explore what kind of atom affords SAA with Ni(111) and Cu(111), neither the larger model than the present one nor the case of $n \geq 5$ was investigated in this work.

In the geometry optimization of $n\text{X}/\text{M}(111)$, the lowest two layers were fixed at their equilibrium positions in the bulk metal and the remaining moiety was relaxed, as shown in Scheme 1 (a). In the SAA, all the X atoms are placed separately on the surface. In the case of $n = 3$ for instance, two kinds of structures are possible, as shown in Scheme 1(b): In one structure, X atoms are separated by one M-M bond and in the other they are separated by one M atom. These two structures are respectively named 3X^{S1} and 3X^{S2} hereinafter, as shown by Scheme 1(b); all other geometries studied here are less stable than these two structures, as

shown in Scheme S1 and Figures S1 to S6 of the SI. In the PSA, all the X atoms are connected with each other. In the case of $n = 3$, X atoms are connected with each other to afford either a triangle cluster or a linear structure on the surface, as illustrated in Scheme 1(c); They are named respectively $3X^{PC}$ and $3X^{PL}$ hereinafter using superscripts “PC” and “PL”; the meaning is described below. The other possible PSA structures were calculated but they were less stable than $3X^{PC}$ or $3X^{PL}$ structures; those structures are shown in Scheme S1 and Figures S1 to S6 of the SI. In $4X/M(111)$, the PL structure is unlikely because it contains an infinite linear X_{∞} moiety on the surface, as shown in Scheme S1 (the right-end of down row) of the SI. Therefore, we did not investigate $4X/M(111)^{PL}$ in this work.



Scheme 1. Pure M(111) surface (a), single-atom alloy (SAA) (b), and phase-separated alloy (PSA) (c), where three X atoms were placed on the M(111) surface as an example and $3X$ represents the presence of three X atoms on the surface. The superscripts “Sn” ($n = 1$ or 2), “PC”, and “PL” of $3X$ respectively represent an SAA form with three dispersed X atoms, a PSA form with a cluster-like X_3 structure, and a PSA form with a linear X_3 structure. The S1 and S2 represent different arrangements of three X atoms.

At the end of this section, we defined abbreviation names of alloys for clarity. The SAA and PSA composed of the n X atoms and M(111) host are named, respectively, $nX/M(111)^S$ and $nX/M(111)^P$, using superscripts “S” and “P”. When the structure of the nX moiety is discussed, the alloys are named $nX/M(111)^{S1}$, $nX/M(111)^{PC}$, and so on hereinafter to represent the geometry of the X_n moiety using superscript, where PC and PL are abbreviations of “PSA” bearing metal atoms in cluster and “PSA” bearing metal atoms on a line.

3. RESULTS AND DISCUSSION

First, we explore possible geometries of SAA and PSA and discuss the most stable geometry in the SAA and PSA. To find determination factor(s) for the SAA and PSA formations, then we compare destabilization energy by removing M atoms from the M(111) surface and stabilization energy by adding either X_n cluster or n X atoms to the M(111) surface bearing the surface deficiencies. Next, we investigate electronic structures of the SAA and PSA such as the Bader charge, Fermi level (ϵ_F), and density of states (DOS). Last, we investigate surface reactivities of the SAA and PSA for CO adsorption, where CO is taken as a probe molecule.

3.1. Structures of Ni(111)-based and Cu(111)-base alloys

To find what kind of element affords SAA with Ni(111) and Cu(111), various geometries were investigated by replacing surface Ni or Cu atoms with X atoms ($X^1 = \text{Cu, Ag, or Au}$ for the Ni(111); $X^2 = \text{Ni, Pd, or Pt}$ for the Cu(111)), as shown in Figures S1 ~ S6 of the SI. The most stable geometries of the SAA and PSA are shown in Figure 1 with several important geometrical parameters.

In the Ni-based alloys, all the Ni–X distances are moderately longer in $nX^1/\text{Ni}(111)^P$ than in $nX^1/\text{Ni}(111)^S$. Also, it is noted that the Ni–X distance increases in the order Ni–Ni < Ni–Cu < Ni–Au < Ni–Ag in both $nX^1/\text{Ni}(111)^S$ and $nX^1/\text{Ni}(111)^P$ and the X^1 – X^1 distance increases in the order of Cu–Cu < Au–Au < Ag–Ag in $nX^1/\text{Ni}(111)^P$. In the Cu-based alloys, the Cu– X^2 distance is moderately longer in $nX^2/\text{Cu}(111)^P$ than in $nX^2/\text{Cu}(111)^S$ except for the Cu–Ni distance, and the Cu– X^2 distance increases in the order Cu–Ni < Cu–Cu < Cu–Pt < Cu–Pd in both $nX^2/\text{Cu}(111)^S$ and $nX^2/\text{Cu}(111)^P$. The Ni–Ni distance of the Ni(111) surface is shorter than the Cu–Cu distance of $n\text{Cu}/\text{Ni}(111)^P$. The Cu–Cu distance of the Cu(111) surface is

longer than the Ni–Ni distance of $n\text{Ni}/\text{Cu}(111)^{\text{P}}$ but considerably shorter than the Pd–Pd distance of $n\text{Pd}/\text{Cu}(111)^{\text{P}}$ and the Pt–Pt distance in $n\text{Pt}/\text{Cu}(111)^{\text{P}}$. All these increasing orders of M–X (M = Ni or Cu) and X–X distances are consistent with the atomic radii of these elements except for the relations between Ag and Au and between Pd and Pt; however, these exceptions are not unreasonable because the atomic radius differs little between them.

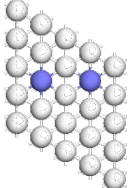
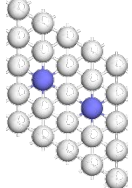
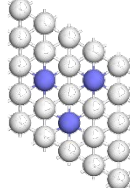
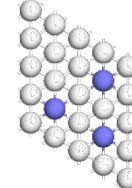
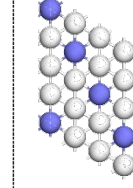
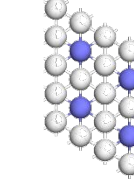
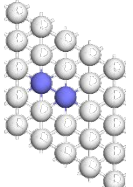
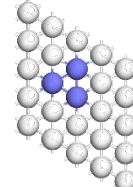
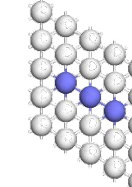
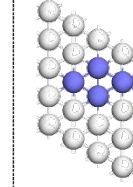
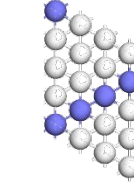
	2X		3X		4X	
SAA						
	2X ^{S1}	2X ^{S2}	3X ^{S1}	3X ^{S2}	4X ^{S1}	4X ^{S2}
$n\text{X}/\text{Ni}(111)$	$\tilde{R}_{\text{M-X}}$	$\tilde{R}_{\text{M-X}}$	$\tilde{R}_{\text{M-X}}$	$\tilde{R}_{\text{M-X}}$	$\tilde{R}_{\text{M-X}}$	$\tilde{R}_{\text{M-X}}$
X=Cu	2.525	2.523	2.522	2.519	2.518	2.515
X=Ag	2.694	2.693	2.710	2.705	2.718	2.708
X=Au	2.639	2.633	2.636	2.624	2.628	2.617
$n\text{X}/\text{Cu}(111)$						
X=Ni	2.530	2.531	2.533	2.535	2.537	2.539
X=Pd	2.607	2.602	2.603	2.593	2.593	2.585
X=Pt	2.593	2.589	2.589	2.582	2.581	2.574
PSA						
	2X ^P		3X ^{PC}	3X ^{PL}	4X ^{PC}	4X ^{PL}
$n\text{X}/\text{Ni}(111)$	$\tilde{R}_{\text{M-X}}/\tilde{R}_{\text{X-X}}$		$\tilde{R}_{\text{M-X}}/\tilde{R}_{\text{X-X}}$	$\tilde{R}_{\text{M-X}}/\tilde{R}_{\text{X-X}}$	$\tilde{R}_{\text{M-X}}/\tilde{R}_{\text{X-X}}$	$\tilde{R}_{\text{M-X}}/\tilde{R}_{\text{X-X}}$
X=Cu	2.530 / 2.505		2.526 / 2.523	2.530 / 2.527	2.525 / 2.522	2.535 / 2.489
X=Ag	2.700 / 2.649		2.709 / 2.694	2.724 / 2.715	2.721 / 2.692	2.780 / 2.569
X=Au	2.658 / 2.666		2.670 / 2.709	2.669 / 2.663	2.683 / 2.707	2.692 / 2.492
$n\text{X}/\text{Cu}(111)$						
X=Ni	2.525 / 2.521		2.529 / 2.494	2.524 / 2.543	2.530 / 2.497	2.515 / 2.566
X=Pd	2.611 / 2.685		2.604 / 2.708	2.611 / 2.632	2.601 / 2.703	2.626 / 2.566
X=Pt	2.598 / 2.674		2.596 / 2.694	2.600 / 2.627	2.596 / 2.688	2.618 / 2.566

Figure 1. The most stable geometries of SAA and PSA of $n\text{X}/\text{M}(111)$ alloys ($\text{X}^1 = \text{Cu}, \text{Ag}, \text{Au}$ for $\text{M} = \text{Ni}$; $\text{X}^2 = \text{Ni}, \text{Pd}, \text{Pt}$ for $\text{M} = \text{Cu}$) in each category. The X atoms are represented using yellow. $\tilde{R}_{\text{M-X}}$ and $\tilde{R}_{\text{X-X}}$ are the averaged values of all the M–X distances and X–X distances, respectively. The surface M–M distance is 2.489 Å on the pure Ni(111) surface and 2.566 Å on the pure Cu(111) surface. The distance between the surface M and the second-layer M is 2.466 Å on the Ni(111) surface and 2.562 Å on the Cu(111) surface.

In the Ni-based alloy of $nX^1/\text{Ni}(111)$, the Cu, Ag, and Au atoms exist at a higher position than the surface Ni atom. In the Cu-based alloy of $nX^2/\text{Cu}(111)$, the Pd and Pt atoms exist at a higher position than the surface Cu atom, whereas the Ni atom exists at a moderately lower position than the surface Cu atom. The position of X is consistent with the atomic radii of the metal atoms. These geometries suggest that the distortion of the M(111) surface increases in the order $\text{Cu} < \text{Ag} \approx \text{Au}$ in $nX^1/\text{Ni}(111)$ and $\text{Ni} < \text{Pt} \approx \text{Pd}$ in $nX^2/\text{Cu}(111)$. The distortion of the Ni(111) surface by X atoms influences the relative stabilities of SAA and PSA because the Ni-X bonding interaction is weakened by the distortion, as discussed below.

3.2. Relative Stabilities of SAA and PSA

Relative stabilities of SAA and PSA are compared in Table 1. In $n\text{Cu}/\text{Ni}(111)$ ($n = 2 \sim 4$), the PSA is more stable than the SAA. In $n\text{Au}/\text{Ni}(111)$ ($n = 2 \sim 4$), on the other hand, the SAA is more stable than the PSA. These findings agree with the previously reported experimental results.^{19,20,25-30} The SAA structure of Au on Ni(111) and the PSA structure of Cu on Ni(111) have been discussed in previously reported computational works,⁵⁶⁻⁵⁸ but the relative stabilities of the SAA and PSA have not been compared before and the reasons why Au atoms form SAA with Ni(111) but Cu atoms form PSA with Ni(111) have been unclear at all. In $n\text{Ag}/\text{Ni}(111)$ ($n = 2 \sim 4$), the relative stabilities depend on the Ag coverage on the Ni(111) surface, as follows; in $2\text{Ag}/\text{Ni}(111)$, the SAA is slightly more stable than the PSA, whereas in $3\text{Ag}/\text{Ni}(111)$ and $4\text{Ag}/\text{Ni}(111)$, the PSA is slightly more stable than the SAA. In $n\text{Pd}/\text{Cu}(111)$ and $n\text{Pt}/\text{Cu}(111)$ ($n = 1$ to 4), the SAA is more stable than the PSA, which agrees with the previously reported experimental results showing that Pt atoms are dispersed separately on Cu nanoparticles at a low ratio of Pt to Cu⁴ and Pd atom is surrounded by Cu atoms at a low loading of Pd.¹⁰ In $2\text{Ni}/\text{Cu}(111)$ and $3\text{Ni}/\text{Cu}(111)$, the SAA is slightly more stable than the PSA, whereas the PSA is more stable than the SAA in $4\text{Ni}/\text{Cu}(111)$. These results are

consistent with the experimental findings showing that the SAA is formed when the Ni content is small (for instance, Ni_{0.001}Cu alloy) but the PSA is formed when the Ni content is large (for instance, Ni_{0.01}Cu alloy).²⁸⁻³⁰ The coverage dependency of relative stabilities of PSA and SAA in nAg/Ni(111) and nNi/Cu(111) is consistent with our intuitive expectation that the alloy tends to have the SAA structure when the content of guest element is small and vice versa. These relative stabilities are summarized in Scheme 2, for easy understanding.

Table 1. Relative energies (eV) of SAA and PSA of nX/M(111) alloys, where a negative value represents a stabilization energy and vice versa.

Alloy Structures ^{a)}			nX/Ni(111)			nX/Cu(111)		
			X = Cu	X = Ag	X = Au	X = Ni	X = Pd	X = Pt
2 X	SAA	2X ^{S1}	0	0	0	0	0	0.007
		2X ^{S2}	0.020	0.070	0.055	0.008	0.019	0
	PSA	2X ^P	-0.013	0.003	0.086	0.006	0.084	0.123
3 X	SAA	3X ^{S1}	0	0	0	0	0	0.028
		3X ^{S2}	0.06	0.174	0.128	0.021	0.051	0
	PSA	3X ^{PC}	-0.032	-0.009	0.188	0.003	0.213	0.314
		3X ^{PL}	-0.023	0.071	0.281	0.023	0.229	0.304
4 X	SAA	4X ^{S1}	0	0	0	0	0	0.038
		4X ^{S2}	0.071	0.206	0.156	0.028	0.061	0
	PSA	4X ^{PC}	-0.109	-0.132	0.229	-0.022	0.328	0.523

a) The superscripts S1, S2, PC, PL etc. are defined in Scheme 1.

In the SAA, the S1 structure is more stable than the S2 except for 2Pt/Cu(111)^S; the S1 and S2 structures are defined in the section of models and shown in Scheme 1 and Figure 1. In the PSA, the PC structure is more stable than the PL except for 3Pt/Cu(111) in which the PL structure is slightly more than the PC. When the PSA is compared with the SAA, the PC structure is employed because the PC is more stable than the PL in almost all cases except for

3Pt/Cu(111) and because even in this exception the energy difference between two structures is tiny.

Ni(111)-based alloy			Cu(111)-based alloy		
	SAA	PSA		SAA	PSA
Cu	x	○		○	x
Ag	○	x		○	x
	x	○		x	○
	x	○		○	x
Au	○	x		○	x

○: stable x: unstable

Scheme 2. Relative stabilities of the SAA and PSA

3.3. Energy changes in formations of SAA and PSA from M(111) and nX atoms

To find the determination factor(s), we analyzed energy changes along assumed reactions to generate either $nX/M(111)^S$ or $nX/M(111)^P$ starting from pure M(111) and nX atoms, as shown in Table 2. In the case of the SAA formation, the first step is to remove n Ni or n Cu atoms from the Ni(111) or Cu(111) surface, respectively. The obtained structure is named $[M(111) - nM]^S$. The energy change E_{rm}^{nS} of this step is defined by eq. (1);

$$E_{rm}^{nS} = E_t[M(111) - nM]_{opt}^S + nE_t(M) - E_t[M(111)]_{opt}, \quad (1)$$

where E_t , n , and the subscript “opt” represent respectively a total energy, a number of M atoms to be removed from the surface, and an optimized structure. The second step is to distort $[M(111) - nM]_{opt}^S$ to the deformed geometry taken to be the same as that in $nX/M(111)^S$. The deformation energy E_{def}^{nS} in this step is defined by eq. (2);

$$E_{def}^{nS} = E_t[M(111) - nM]_{def}^S - E_t[M(111) - nM]_{opt}^S, \quad (2)$$

where the subscript “def” means that the geometry of $[M(111) - nM]^S$ is deformed like that in $nX/M(111)^S$. The final step is to add n X atoms to the surface of the $[M(111) - nM]_{def}^S$ host. In this step, the stabilization energy E_{int}^{nS} is obtained, as represented by eq. (3);

$$E_{\text{int}}^{\text{nS}} = E_{\text{t}}[\text{nX/M(111)}^{\text{S}}] - E_{\text{t}}[\text{M(111)} - \text{nX}]_{\text{def}}^{\text{S}} - nE_{\text{t}}(\text{X}). \quad (3)$$

The sum of these three terms, $\Delta E_{\text{tot}}^{\text{nS}}$, corresponds to a total energy change to produce $\text{nX/M(111)}^{\text{S}}$ from M(111) and nX atoms;

$$\Delta E_{\text{tot}}^{\text{nS}} = E_{\text{rm}}^{\text{nS}} + E_{\text{def}}^{\text{nS}} + E_{\text{int}}^{\text{nS}}. \quad (4)$$

Its negative value represents a stabilization energy of the sum of $\text{nX/M(111)}^{\text{S}}$ and n M atoms relative to the sum of M(111) and n X atoms; it is noted that its positive value does not mean that the SAA cannot be produced, because eq. (4) does not involve all the stabilization energies; for instance, a cohesive energy of n M atoms is not considered here; the reason is presented in note 59. Here, the $\Delta E_{\text{tot}}^{\text{nS}}$ value is used to discuss the relative stabilities of the SAA and PSA.

In the case of the PSA formation, the first step is to remove either a Ni_n or Cu_n cluster from the Ni(111) or Cu(111) surface, respectively, where n Ni or n Cu atoms are connected with each other. This structure is named $[\text{M(111)} - \text{M}_n]^{\text{P}}$. The energy change $E_{\text{rm}}^{\text{nP}}$ is evaluated by eq. (5):

$$E_{\text{rm}}^{\text{nP}} = E_{\text{t}}[\text{M(111)} - \text{M}_n]_{\text{opt}}^{\text{P}} + E_{\text{t}}(\text{M}_n)_{\text{def}} - E_{\text{t}}[\text{M(111)}]_{\text{opt}}, \quad (5)$$

where M_n represents a cluster composed of n M atoms and the subscript “def” means that the M_n cluster has the same geometry as that in the M(111) surface; note that the optimized structure of the M_n cluster is not used in this assumed reaction. The second step is to dissociate the M_n cluster into n M atoms. The dissociation energy $E_{\text{dis,Mn}}^{\text{nP}}$ of the M_n cluster is defined by eq. (6):

$$E_{\text{dis,Mn}}^{\text{nP}} = nE_{\text{t}}(\text{M}) - E_{\text{t}}(\text{M}_n)_{\text{def}}. \quad (6)$$

The next step is to distort $[\text{M(111)} - \text{M}_n]_{\text{opt}}^{\text{P}}$ to the deformed geometry which is the same as the corresponding moiety in $\text{nX/M(111)}^{\text{P}}$. This deformation energy $E_{\text{def}}^{\text{nP}}$ is defined by eq. (7);

$$E_{\text{def}}^{\text{nP}} = E_{\text{t}}[\text{M(111)} - \text{M}_n]_{\text{def}}^{\text{P}} - E_{\text{t}}[\text{M(111)} - \text{M}_n]_{\text{opt}}^{\text{P}}, \quad (7)$$

where the subscript “def” means that the geometry of $[M(111) - M_n]^P$ is deformed like that in $nX/M(111)^P$. This eq. resembles the eq. (2). Then, we define the formation energy E_{f,X_n}^{nP} of X_n cluster from n X atoms, using eq. (8);

$$E_{f,X_n}^{nP} = E_t(X_n)_{\text{def}} - nE_t(X), \quad (8)$$

where X_n represents a cluster consisting of n X atoms and the subscript “def” means that the X_n cluster has the same deformed geometry as that in $nX/M(111)^P$. The last step is to add the X_n cluster to $[M(111) - M_n]_{\text{def}}^P$. The interaction energy E_{int}^{nP} is defined by eq. (9);

$$E_{\text{int}}^{nP} = E_t[nX/M(111)^P] - E_t[M(111) - M_n]_{\text{def}}^P - E_t(X_n)_{\text{def}}. \quad (9)$$


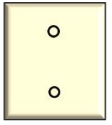
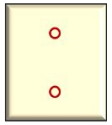
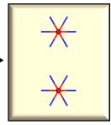


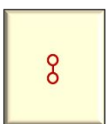
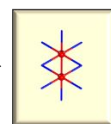
The sum of these five terms, $\Delta E_{\text{tot}}^{nP}$, corresponds to a total energy change to produce $nX/M(111)^P$ from $M(111)$ and nX atoms:

$$\Delta E_{\text{tot}}^{nP} = E_{\text{rm}}^{nP} + E_{\text{dis},M_n}^{nP} + E_{\text{def}}^{nP} + E_{f,X_n}^{nP} + E_{\text{int}}^{nP}. \quad (10)$$

The E_{rm}^{nS} term in the SAA formation case corresponds to the $E_{\text{rm}}^{nP} + E_{\text{dis},M_n}^{nP}$ term in the PSA formation case, because these two terms represent the destabilization energy by the conversion of $M(111)$ to either $[M(111) - nM]_{\text{opt}}^S + nM$ in the SAA case or $[M(111) - M_n]_{\text{opt}}^P + nM$ in the PSA case. Also, the E_{int}^{nS} term in the SAA case corresponds to the $E_{f,X_n}^{nP} + E_{\text{int}}^{nP}$ term in the PSA case, because these two terms represent the stabilization energy by the formation of either $nX/M(111)^S$ or $nX/M(111)^P$ from n X atoms and either $[M(111) - nM]_{\text{def}}^S$ or $[M(111) - M_n]_{\text{def}}^P$, respectively.

As shown in Table 2, the $\Delta E_{\text{tot}}^{2S}$ term is more positive than the $\Delta E_{\text{tot}}^{2P}$ term in $2\text{Cu}/\text{Ni}(111)$, while the $\Delta E_{\text{tot}}^{2S}$ term is less positive than the $\Delta E_{\text{tot}}^{2P}$ term in $2\text{Au}/\text{Ni}(111)$. These $\Delta E_{\text{tot}}^{2S}$ and $\Delta E_{\text{tot}}^{2P}$ values indicate that the PSA is more stable than the SAA in $2\text{Cu}/\text{Ni}(111)$ but the SAA is more stable than the PSA in $2\text{Au}/\text{Ni}(111)$. This conclusion is the same as that shown in Table 1 and Scheme 2. Thus, the $\Delta E_{\text{tot}}^{2S}$ and $\Delta E_{\text{tot}}^{2P}$ terms are useful for finding the reason(s) why $2\text{Cu}/\text{Ni}(111)$ forms the PSA but $2\text{Au}/\text{Ni}(111)$ forms the SAA.

Table 2. Energy changes along the assumed procedure to form the most stable SAA and PSA structures^{a)} of 2X/M(111) from M(111) and 2X atoms

		M(111)	$[M(111)-2M]_{opt}^S$	$[M(111)-2M]_{def}^S$	$2X/M(111)^S$			
			$-2M$ → 	deform → 	$+2X$ → 	SAA		
		X	$E_{rm}^{2S\ b)}$	$E_{def}^{2S\ b)}$	$E_{int}^{2S\ b)}$	ΔE_{tot}^{2S}		
Ni(111)	M		11.748	0.059	-9.368	2.439		
	Ag		11.748	0.089	-7.183	4.654		
	Au		11.748	0.115	-9.180	2.683		
Cu(111)	M		8.090	0.074	-10.850	-2.686		
	Pd		8.090	0.084	-10.109	-1.935		
	Pt		8.022 ^{c)}	0.192	-13.922	-5.708		
		M(111)	$[M(111)-2M]_{opt}^P$	$[M(111)-M_2]_{def}^P$	$2X/M(111)^P$			
			$-2M$ → 	M_2 → $2M$ → 	$2X$ → X_2 → 	PSA		
		X	$E_{rm}^{2P\ d)}$	$E_{dis,M_2}^{2P\ d)}$	$E_{def}^{2P\ d)}$	$E_{f,X_2}^{2P\ d)}$	$E_{int}^{2P\ d)}$	ΔE_{tot}^{2P}
Ni(111)	M		9.020	2.381	0.112	-2.023	-7.094	2.396
	Ag		9.020	2.381	0.102	-1.759	-5.088	4.656
	Au		9.020	2.381	0.199	-2.232	-6.630	2.738
Cu(111)	M		5.881	1.939	0.117	-2.262	-8.355	-2.680
	Pd		5.881	1.939	0.104	-1.180	-8.595	-1.851
	Pt		5.881	1.939	0.176	-2.960	-10.622	-5.586

a) The most stable structure presented in Table 1 is employed here. b) E_{rm}^{2S} , E_{def}^{2S} , and E_{int}^{2S} terms are respectively defined by eqs. (1), (2), and (3). c) This value differs from the E_{rm}^{2S} values of 2Ni/Cu(111) and 2Pd/Cu(111) because 2Pt/Cu(111) has the S2 structure in which two Pt atoms are separated by one Cu atom but 2Ni/Cu(111) and 2Pd/Cu(111) have the S1 structure in which two X atoms (X = Ni or Pd) are separated by one Cu-Cu bond, as shown in Table 1, Scheme 1, and Scheme S3 of the SI. d) E_{rm}^{2P} , E_{dis,M_2}^{2P} , E_{f,X_2}^{2P} , and E_{int}^{2P} terms are respectively defined by eqs. (5), (6), (7), (8) and (9). All these terms are in eV unit.

3.4. Comparison between SAA and PSA formations

First, we explain the overview of Table 2, where 2X/Ni(111) case is shown because this is the simplest alloy. In all the combinations studied, the destabilization energy term $E_{\text{rm}}^{2\text{S}}$ in the SAA case is larger than the $E_{\text{rm}}^{2\text{P}} + E_{\text{dis},\text{M}_2}^{2\text{P}}$ term in the PSA case. This is reasonable because more M-M bonds are broken in $[\text{M}(111) - 2\text{M}]_{\text{opt}}^{\text{S}}$ than in $[\text{M}(111) - \text{M}_2]_{\text{opt}}^{\text{P}}$; note that the $E_{\text{rm}}^{2\text{S}}$ value of 2Pt/Cu(111)^{S1} moderately differs from those of 2Ni/Cu(111)^{S2} and 2Pd/Cu(111)^{S2} because 2Pt/Cu(111)^{S1} has a different structure from those of 2Ni/Cu(111)^{S2} and 2Pd/Cu(111)^{S2}, as explained in footnote c) of Table 2. The deformation energy $E_{\text{def}}^{2\text{P}}$ in the PSA case is moderately larger than the $E_{\text{def}}^{2\text{S}}$ in the SAA case except for nPt/Cu(111). The stabilization energy $E_{\text{int}}^{2\text{S}}$ in the SAA case is always larger than the sum of $E_{\text{f},\text{X}_2}^{2\text{P}}$ and $E_{\text{int}}^{2\text{P}}$ in the PSA case, as shown in Table 2. This is reasonable because 18 M-X bonds (12 M-X bonds on the surface and 6 M-X bonds between the surface and the second layers) are formed by this step in the SAA case but in the PSA case 16 M-X bonds (10 M-X bonds on the surface and 6 M-X bonds between the surface and the second layers) and one X-X bond are formed. These are common features in all the alloys studied here. However, the simple inspection into these terms does not provide us with the reason(s) why 2Cu/Ni(111) forms the PSA but 2Au/Ni(111) forms the SAA.

In 2Cu/Ni(111), the $E_{\text{rm}}^{2\text{S}}$ term is more positive than the $E_{\text{rm}}^{2\text{P}} + E_{\text{dis},\text{M}_2}^{2\text{P}}$ term by 0.347 eV, as shown in Table 2. Although the $E_{\text{def}}^{2\text{S}}$ term is moderately less positive than the $E_{\text{def}}^{2\text{P}}$ term by 0.053 eV, the $E_{\text{int}}^{2\text{S}}$ term is more negative than the $E_{\text{f},\text{X}_2}^{2\text{P}} + E_{\text{int}}^{2\text{P}}$ term by 0.251 eV. Thus, it is concluded that the $E_{\text{int}}^{2\text{S}}$ term does not overcome the large destabilization energy by the $E_{\text{rm}}^{2\text{S}}$, and the PSA is more stable than the SAA. When going from 2Cu/Ni(111) to 2Au/Ni(111), the $E_{\text{def}}^{2\text{S}}$ term gets more positive by 0.056 eV in the SAA but the $E_{\text{def}}^{2\text{P}}$ term gets more positive by 0.087 eV in the PSA (Table 2), indicating that the E_{def} term favors the SAA formation. The $E_{\text{int}}^{2\text{S}}$ term gets less negative by 0.188 eV in the SAA, whereas the $E_{\text{f},\text{X}_2}^{2\text{P}} + E_{\text{int}}^{2\text{P}}$ term gets less negative by 0.255 eV in the PSA. Because the $E_{\text{f},\text{X}_2}^{2\text{P}}$ term gets more

negative by 0.209 eV but the $E_{\text{int}}^{2\text{P}}$ term gets less negative by 0.464 eV, the $E_{\text{int}}^{2\text{P}}$ term plays a dominant role in decreasing the $E_{\text{f},\text{X}_2}^{2\text{P}} + E_{\text{int}}^{2\text{P}}$ term. Both the larger decrease in the $E_{\text{f},\text{X}_2}^{2\text{P}} + E_{\text{int}}^{2\text{P}}$ term than that in the $E_{\text{int}}^{2\text{S}}$ term and the larger increase in the $E_{\text{def}}^{2\text{P}}$ term than that in the $E_{\text{def}}^{2\text{S}}$ term destabilize $2\text{Au}/\text{Ni}(111)^{\text{P}}$ more than $2\text{Au}/\text{Ni}(111)^{\text{S}}$. Because the change in the $E_{\text{def}}^{2\text{P}}$ term is much smaller than that in the $E_{\text{f},\text{X}_2}^{2\text{P}} + E_{\text{int}}^{2\text{P}}$ term, it is concluded that the most important factor for destabilizing $2\text{Au}/\text{Ni}(111)^{\text{P}}$ relative to $2\text{Au}/\text{Ni}(111)^{\text{S}}$ is the larger decrease in the $E_{\text{f},\text{X}_2}^{2\text{P}} + E_{\text{int}}^{2\text{P}}$ term than in the $E_{\text{int}}^{2\text{S}}$ term when going from $\text{X} = \text{Cu}$ to $\text{X} = \text{Au}$. As a result, $2\text{Au}/\text{Ni}(111)$ forms the SAA.

When going from $2\text{Cu}/\text{Ni}(111)$ to $2\text{Ag}/\text{Ni}(111)$, the $E_{\text{def}}^{2\text{S}}$ term gets more positive by 0.030 eV but the $E_{\text{def}}^{2\text{P}}$ term gets less positive by 0.010 eV, as shown in Table 2, indicating that the E_{def} term facilitates the PSA formation by 0.040 eV compared to the SAA formation. The $E_{\text{int}}^{2\text{S}}$ term gets less negative by 2.185 eV, but the $E_{\text{f},\text{X}_2}^{2\text{P}} + E_{\text{int}}^{2\text{P}}$ term gets less negative by 2.270 eV, indicating that these terms facilitate the SAA formation by 0.085 eV compared to the PSA formation. This energy difference (0.085 eV) is larger than that (0.04 eV) by the $E_{\text{def}}^{2\text{S}}$ and $E_{\text{def}}^{2\text{P}}$ terms. Therefore, the $E_{\text{int}}^{2\text{S}}$ term facilitates the SAA formation compared to the PSA formation when going from $2\text{Cu}/\text{Ni}(111)$ to $2\text{Ag}/\text{Ni}(111)$. As a result, $2\text{Ag}/\text{Ni}(111)^{\text{S}}$ becomes as stable as $2\text{Ag}/\text{Ni}(111)^{\text{P}}$ (Table 2) unlike $2\text{Cu}/\text{Ni}(111)$ in which the PSA is more stable than the SAA. These results indicate that the $E_{\text{int}}^{2\text{S}}$ term plays a more important role in stabilizing the SAA than does the E_{def} term.

In $2\text{Ni}/\text{Cu}(111)$, the smaller $E_{\text{def}}^{2\text{S}}$ term than the $E_{\text{def}}^{2\text{P}}$ term and the more negative $E_{\text{int}}^{2\text{S}}$ term than the $E_{\text{int}}^{2\text{P}} + E_{\text{f},\text{X}_2}^{2\text{P}}$ term almost compensate the larger $E_{\text{rm}}^{2\text{S}}$ term than the $E_{\text{rm}}^{2\text{P}}$ term (Table 2). Therefore, $2\text{Ni}/\text{Cu}(111)^{\text{S}}$ is as stable as $2\text{Ni}/\text{Cu}(111)^{\text{P}}$. When going from $2\text{Ni}/\text{Cu}(111)$ to $2\text{Pd}/\text{Cu}(111)$, the $E_{\text{def}}^{2\text{S}}$ term moderately increases, whereas the $E_{\text{def}}^{2\text{P}}$ term is moderately decreases. However, these changes are not large, indicating that these terms do not contribute significantly to the relative stabilities of the SAA and PSA. On the other hand, the

$E_{\text{int}}^{2\text{S}}$ and $E_{\text{int}}^{2\text{P}} + E_{\text{f},\text{X}_2}^{2\text{P}}$ terms get considerably less negative by 0.741 eV and 0.842 eV, respectively. The change in the $E_{\text{int}}^{2\text{P}} + E_{\text{f},\text{X}_2}^{2\text{P}}$ term is larger than in the $E_{\text{int}}^{2\text{S}}$ term by 0.101 eV. As a result, $2\text{Pd}/\text{Cu}(111)^{\text{P}}$ becomes less stable than $2\text{Pd}/\text{Cu}(111)^{\text{S}}$. It is worthy to note that the $E_{\text{int}}^{2\text{S}}$ term plays an important role for stabilizing the SAA compared to the PSA in the $2\text{Pd}/\text{Cu}(111)$ case, too.

Table 3. The assumed procedure to form the SAA and PSA structures ^{a)} of $4\text{X}/\text{M}(111)$ from $\text{M}(111)$ and 4X atoms

		$\text{M}(111)$	$[\text{M}(111)-4\text{M}]_{\text{opt}}^{\text{S}}$	$[\text{M}(111)-4\text{M}]_{\text{def}}^{\text{S}}$	$4\text{X}/\text{M}(111)^{\text{S}}$			
						SAA		
		X	$E_{\text{rm}}^{4\text{S b)}$	$E_{\text{def}}^{4\text{S b)}$	$E_{\text{int}}^{4\text{S b)}$	$\Delta E_{\text{tot}}^{4\text{S}}$		
Ni(111)	M		23.454	0.305	-18.847	4.912		
	Ag		23.454	0.264	-14.093	9.652		
	Au		23.454	0.434	-18.202	5.686		
Cu(111)	M		16.606	0.108	-21.534	-4.820		
	Pd		16.606	0.179	-20.039	-3.254		
	Pt		16.268 ^{c)}	0.380	-27.502	-10.854		
		$\text{M}(111)$	$[\text{M}(111)-4\text{M}]_{\text{opt}}^{\text{P}}$	$[\text{M}(111)-\text{M}_4]_{\text{def}}^{\text{P}}$	$4\text{X}/\text{M}(111)^{\text{P}}$			
						PSA_C		
		X	$E_{\text{rm}}^{4\text{P d)}$	$E_{\text{dis},\text{M}_4}^{4\text{P d)}$	$E_{\text{def}}^{4\text{P d)}$	$E_{\text{f},\text{X}_4}^{4\text{P d)}$	$E_{\text{int}}^{4\text{P d)}$	$\Delta E_{\text{tot}}^{4\text{P}}$
Ni(111)	M		13.986	7.845	0.162	-5.942	-11.248	4.804
	Ag		13.986	7.845	0.215	-4.428	-8.125	9.494
	Au		13.986	7.845	0.287	-6.036	-10.167	5.916
Cu(111)	M		9.469	5.886	0.167	-7.809	-12.554	-4.841
	Pd		9.469	5.886	0.142	-5.637	-12.787	-2.927
	Pt		9.469	5.886	0.256	-10.101	-15.841	-10.331

a) The most stable structure presented in Table 1 is employed here. b) $E_{\text{rm}}^{4\text{S}}$, $E_{\text{def}}^{4\text{S}}$, and $E_{\text{int}}^{4\text{S}}$ are defined by eqs. (1), (2), and (3). c) This value differs from the $E_{\text{rm}}^{4\text{S}}$ values of $4\text{Ni}/\text{Cu}(111)$ and $4\text{Pd}/\text{Cu}(111)$ because $4\text{Pt}/\text{Cu}(111)$ has the S2 structure in which two Pt atoms are separated by one Cu atom but $4\text{Ni}/\text{Cu}(111)$ and $4\text{Pd}/\text{Cu}(111)$ have the S1 structure in which two X atoms ($\text{X} = \text{Ni}$ or Pd) are separated by one Cu-Cu bond and other two X atoms are separated by one Cu atom, as shown in Table 1, Scheme 1, and Scheme S3 of the SI. d) $E_{\text{rm}}^{4\text{P}}$, $E_{\text{dis},\text{M}_4}^{4\text{P}}$, $E_{\text{f},\text{X}_4}^{4\text{P}}$, and $E_{\text{int}}^{4\text{P}}$ are defined by eqs. (5), (6), (7), (8) and (9). All these terms are in eV unit.

When going from 2Ni/Cu(111) to 2Pt/Cu(111), the $E_{\text{def}}^{2\text{S}}$ term gets more positive by 0.116 eV but the $E_{\text{def}}^{2\text{P}}$ term gets more positive by 0.064 eV, indicating that these terms contribute to stabilizing 2Pt/Cu(111)^P compared to 2Pt/Cu(111)^S by 0.052 eV. On the other hand, the $E_{\text{int}}^{2\text{S}}$ term gets more negative by 3.072 eV, and the $E_{\text{int}}^{2\text{P}} + E_{\text{f},\text{X}2}^{2\text{P}}$ term gets more negative by 2.965 eV, indicating that the $E_{\text{int}}^{2\text{S}}$ term contributes to stabilizing 2Pt/Cu(111)^S compared to 2Pt/Cu(111)^P by 0.107 eV. Because the contribution of the $E_{\text{int}}^{2\text{S}}$ is larger than that of $E_{\text{def}}^{2\text{P}}$, 2Pt/Cu(111)^S is more stable than 2Pt/Cu(111)^P. These results again indicate that the $E_{\text{int}}^{2\text{S}}$ term is important in stabilizing the SAA compared to the PSA.

Similar analysis is possible for 3X/Ni(111) and 4X/Ni(111). Here, we presented these terms of 4X/Ni(111) in Table 3 without discussion; the discussion is presented in pages S15 to S20 of the SI and these terms of 3X/Ni(111) and 4X/Ni(111) are shown in Tables S4 and S5 of the SI.

In summary, the interaction energy E_{int} between $n\text{X}$ atoms and $[\text{M}(111) - n\text{M}]_{\text{def}}^{\text{S}}$ and that between X_n cluster and $[\text{M}(111) - \text{M}_n]_{\text{def}}^{\text{P}}$ are determination factors for relative stabilities of SAA and PSA. Thus, important is to find what property determines the E_{int} value, which is discussed in the section 3.6.

3.5. Electronic structures of SAA and PSA

Prior to discussing the E_{int} term, we investigate here the Bader charge, the Fermi level (ε_{F}), and d -band center (ε_{dc}) of $n\text{X}/\text{M}(111)$ because these are important properties of the metal surface and because these properties are necessary for discussing the E_{int} term.

In $n\text{Cu}/\text{Ni}(111)^{\text{S}}$ and $n\text{Cu}/\text{Ni}(111)^{\text{P}}$, the Cu atom has a slightly positive charge, as shown in Figure 2. However, the Ag and Au atoms are negatively charged and the atomic charge gets more negative in the order $\text{Ag} < \text{Au}$ in both the PSA and SAA. In $n\text{X}/\text{Cu}(111)^{\text{S}}$ and $n\text{X}/\text{Cu}(111)^{\text{P}}$ ($\text{X} = \text{Ni}, \text{Pd}, \text{or Pt}$), Ni, Pd, and Pt atoms are negatively charged and the atomic charge gets more negative in the order $\text{Ni} \leq \text{Pd} < \text{Pt}$ (Figure 2). These trends are reasonable

because the electronegativity increases in the same order. It is also noteworthy that the ε_F lowers in energy in the order $X = \text{Cu} \sim \text{Ag} > \text{Au}$ in $nX/\text{Ni}(111)^S$ and $nX/\text{Ni}(111)^P$ and $X = \text{Ni} \sim \text{Pd} > \text{Pt}$ in $nX/\text{Cu}(111)^S$ and $nX/\text{Cu}(111)^P$, which is discussed below in more detail.

Each X atom is more negatively charged in the SAA than in the PSA, as seen in Figure 2 and Tables S6 and S7 of the SI, except for the case of $n\text{Cu}/\text{Ni}(111)$ in which the Cu atomic charge differs little between the SAA and PSA. This result is reasonable because each X atom in $nX/M(111)^S$ interacts with more M atoms than in $nX/M(111)^P$ and the charge transfer (CT) between the X atom and the M(111) host occurs more strongly in the SAA than in the PSA.

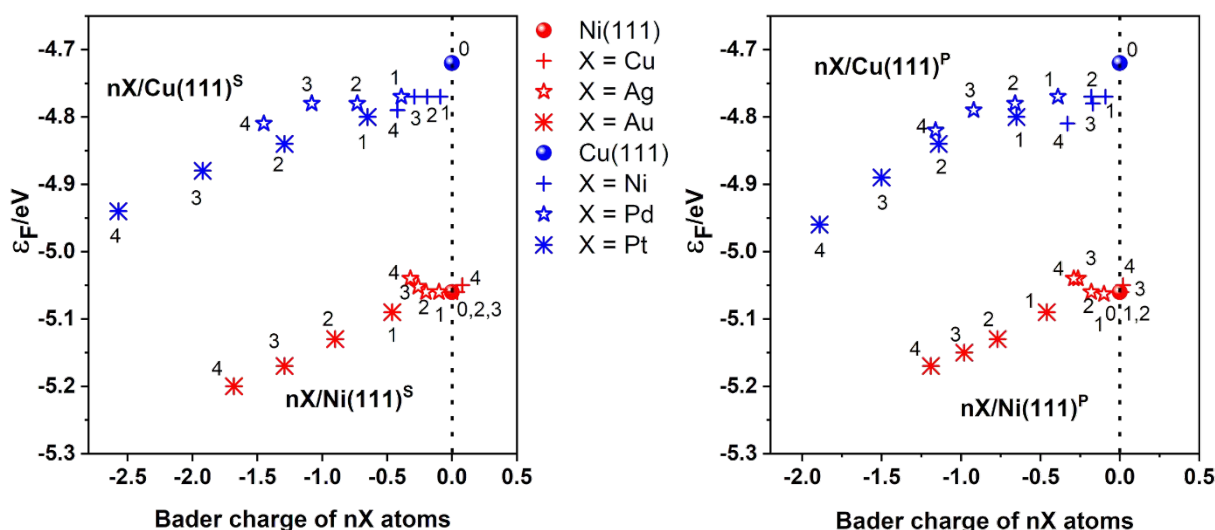


Figure 2. Relations between the Fermi level (ε_F in eV) and the Bader charge (in e) of nX atoms or X_n cluster in $nX/M(111)^S$ (a) and $nX/M(111)^P$ ($n = 0 \sim 4$) (b). The number neighboring each plot represents the number of X atoms in the alloy.

The ε_F of the alloy lowers in energy as the negative charge of dopant metals increases, as shown in Figure 2, except for $n\text{Ag}/\text{Ni}(111)$. This is reasonable because more negatively charged dopant metals means that the host has positive charge and therefore the ε_F value lowers in energy. It is noted that the ε_F value of $n\text{Cu}/\text{Ni}(111)$ differs little from that of Ni(111), as shown in Figure 2 and Table 4. This is not unreasonable because of the reasons below; (i) the CT occurs very weakly in this alloy, as discussed above, (ii) the amount of Cu is not

large, and (iii) the Cu atoms exist on the surface but the ε_F is determined by the whole metal atoms in the alloy. In the case of 2Ag/Ni(111) and 3Ag/Ni(111), the ε_F value is almost equal to that of Ni(111) despite of the moderately negative charge of the Ag atoms (Table 4). In 3Ag/Ni(111) and 4Ag/Ni(111), the ε_F rises slightly by 0.02 eV compared to that of Ni(111). In nAg/Ni(111), the CT is not very strong. Therefore, it is likely that the other factor such as structure distortion influences the ε_F value because the larger Ag atom than the Ni atom induces the distortion of the host Ni(111) structure to destabilize the d band of Ni(111) and rise the ε_F value; we stop the further discussion about this issue because the change in the ε_F is very small. On the other hand, it lowers considerably in nAu/Ni(111) as the number of Au atoms increases because the CT occurs considerably from Ni(111) to Au atoms. Similarly, the ε_F value lowers considerably in nPt/Cu(111) as the number of Pt atoms increases because of the same reason. From these results, it is concluded that the Fermi level lowers in energy when CT from host metals to dopant atoms strongly occurs but the other factor would influence the Fermi level when the CT is weak; also, the interface dipole moment is another factor to influence the Fermi level, but this factor is not discussed here because it is difficult to define the interface dipole moment due to the SAA structure in which dopant metals are surrounded by host metal atoms.

Because the surface of the alloy plays important roles in adsorption of gas molecule and reaction of substrate, we inspect the partial DOS (PDOS) of the top-layer (or the surface layer) of the PSA and SAA, as shown in Figure 3, where several important PDOSs are presented as examples; PDOSs of the other alloys are shown in Figures S7 ~ S14 of the SI. The PDOS of the top-layer of Ni(111) exhibits spin-polarization but that of the Cu(111) surface does not. These features are found in all the nX/Ni(111) and nX/Cu(111) alloys. In the PDOS of Ni(111), the Ni β -electron d -DOS mainly contributes to the ε_F . This feature is common in all the nX/Ni(111) alloys studied here. In the PDOS of Cu(111), both the Cu d -DOS and the Cu

s -DOS are small around the Fermi level. In $nX/Cu(111)$, the DOS becomes further smaller at the Fermi level. This is true because the Cu DOS at a high energy more contributes to the CT to Ni, Pd, and Pt atoms than that at a low energy.

The d band center (ε_{dc-tot} , eV) and d valence-band center (ε_{dc-vb}) are important properties as well. We focus on these properties of the surface top-layer. In the Ni-based alloy, the ε_{dc-tot} and

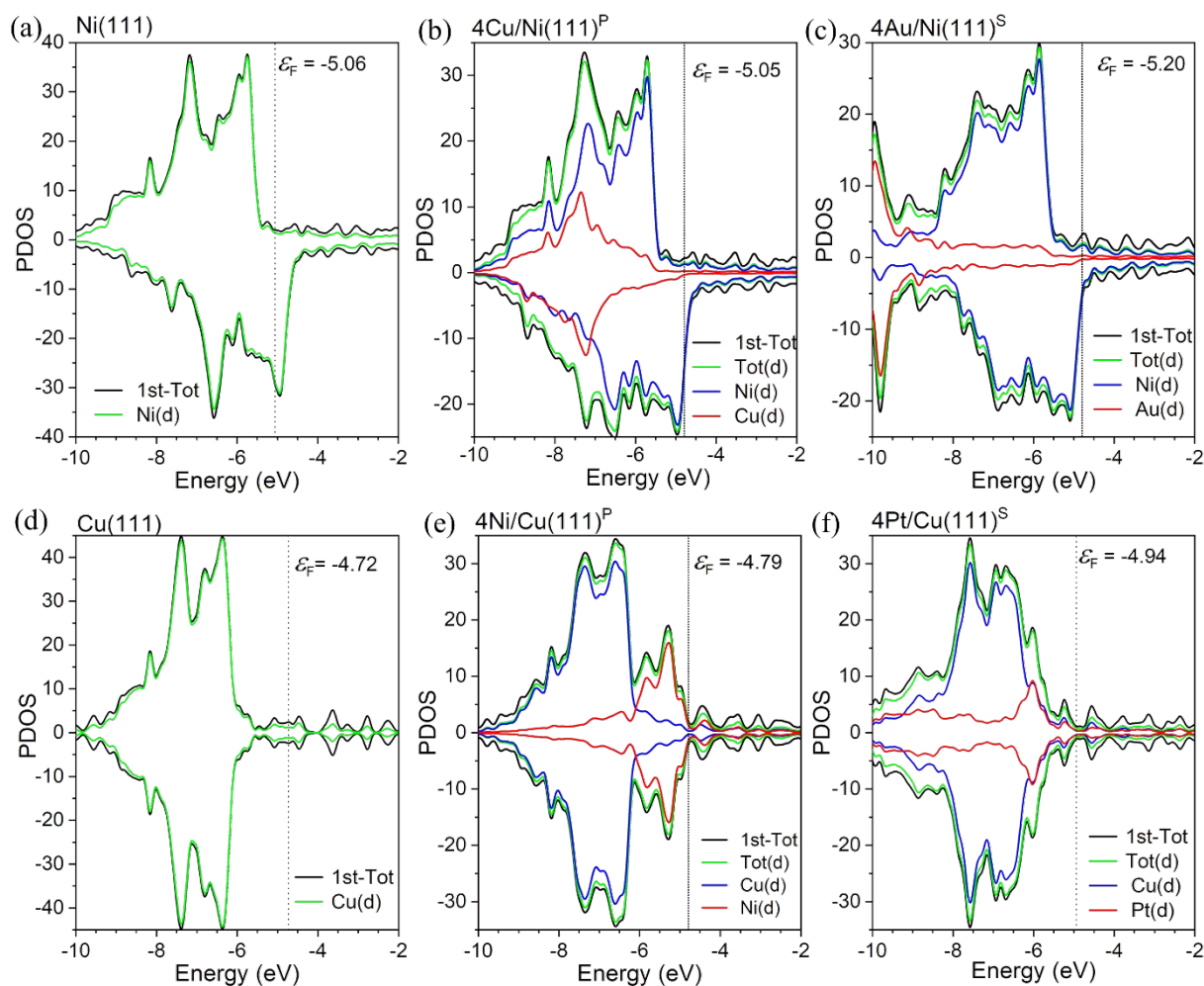


Figure 3. The PDOSs of the top-layer (or the surface layer) of Ni(111) (a), 4Cu/Ni(111)^P (b), 4Au/Ni(111)^S (c), Cu(111) (d), 4Ni/Cu(111)^P (e), and 4Pt/Cu(111)^S (f). The PDOSs of the other alloys are presented in Figures S7 ~ S14 of the SI.

ε_{dc-vb} lower in energy as going from Ni(111) to $nX/Ni(111)$, as shown in Table 4; the properties of the other alloys are presented in Table S8 of the SI. These changes in ε_{dc-tot} and ε_{dc-vb} suggest that the CT from $nX/Ni(111)$ to adsorbate weakens as going from Ni(111) to

nX/Ni(111). We find one question here about the reason why the $\epsilon_{\text{dc-tot}}$ and $\epsilon_{\text{dc-VB}}$ values lower as going from Ni(111) to nCu/Ni(111). The CT from the Cu atoms to the Ni(111) host is not the reason because the CT is marginal in nCu/Ni(111), as discussed above and seen in Figure 2. One plausible reason is the contribution of the d valence bands of the Cu atom and Cu_n cluster to the $\epsilon_{\text{dc-tot}}$ and $\epsilon_{\text{dc-VB}}$. Their d valence bands exist at a much lower energy than that of Ni(111), as shown in Figure 3(b). Also, the extent of the Cu d valence band at a low energy is much larger in $4\text{Cu}/\text{Ni}(111)^{\text{P}}$ than in $\text{Cu}/\text{Ni}(111)$, as shown by the PDOSs of $\text{Cu}/\text{Ni}(111)$ (Figures S7 of the SI) and $4\text{Cu}/\text{Ni}(111)^{\text{P}}$ (Figure 3(b)). Therefore, the increase in the Cu content enhances the contribution of the low energy d band to the $\epsilon_{\text{dc-tot}}$ and $\epsilon_{\text{dc-VB}}$. As a result, the $\epsilon_{\text{dc-tot}}$ and $\epsilon_{\text{dc-VB}}$ values lower in energy as the number of Cu atoms increases in nCu/Ni(111) despite of the marginal CT.

Table 4. The Fermi level (ϵ_{F} in eV), d band center ($\epsilon_{\text{d-tot}}$ in eV), and d band center in the valence level ($\epsilon_{\text{d-VB}}$ in eV) of nX/Ni(111) and nX/Cu(111) alloys

nX ¹ /Ni(111)	ϵ_{F}	$\epsilon_{\text{dc-tot}}$	$\epsilon_{\text{dc-VB}}$	nX ² /Cu(111)	ϵ_{F}	$\epsilon_{\text{dc-tot}}$	$\epsilon_{\text{dc-VB}}$
nX ¹	[nCu/Ni(111)] ^P			nX ²	[nNi/Cu(111)] ^P		
none	-5.06	-4.71	-6.77	none	-4.72	-5.92	-7.19
Cu	-5.06	-4.76	-6.80	Ni	-4.77	-5.91	-7.15
2Cu ^P	-5.06	-4.84	-6.85	2Ni ^P	-4.77	-5.85	-7.13
3Cu ^{PC}	-5.06	-4.90	-6.88	3Ni ^{PC}	-4.78	-5.71	-7.02
4Cu ^{PC}	-5.05	-4.97	-6.91	4Ni ^{PC}	-4.81	-5.57	-6.92
	[nAg/Ni(111)] ^P				[nPd/Cu(111)] ^S		
Ag	-5.06	-4.81	-6.88	Pd	-4.77	-5.96	-7.23
2Ag ^P	-5.06	-4.99	-7.10	2Pd ^{S1}	-4.78	-5.94	-7.29
3Ag ^{PC}	-5.04	-5.15	-7.26	3Pd ^{S1}	-4.78	-5.82	-7.22
4Ag ^{PC}	-5.04	-5.30	-7.41	4Pd ^{S1}	-4.81	-5.73	-7.19
	[nAu/Ni(111)] ^S				[nPt/Cu(111)] ^S		
Au	-5.09	-4.87	-6.95	Pt	-4.80	-6.00	-7.27
2Au ^{S1}	-5.13	-5.04	-7.14	2Pt ^{S2}	-4.84	-6.02	-7.37

3Au ^{S1}	-5.17	-5.21	-7.32	3Pt ^{S2}	-4.88	-6.05	-7.49
4Au ^{S1}	-5.20	-5.38	-7.48	4Pt ^{S2}	-4.94	-5.89	-7.37

In the Cu-based alloy nNi/Cu(111)^S, on the other hand, the $\epsilon_{\text{dc-tot}}$ and $\epsilon_{\text{dc-VB}}$ rise in energy as going from Cu(111) to 4Ni/Cu(111)^S. In nPd/Cu(111)^S, the $\epsilon_{\text{dc-tot}}$ moderately but the $\epsilon_{\text{dc-VB}}$ slightly rise in energy when going from Pd/Cu(111) to 4Pd/Cu(111). In nPt/Cu(111)^S, on the other hand, the $\epsilon_{\text{dc-tot}}$ and $\epsilon_{\text{dc-VB}}$ moderately lower in energy when going from Pt/Cu(111) to 3Pt/Cu(111)^S but then rise when going to 4Pt/Cu(111)^S. These complex changes in $\epsilon_{\text{dc-tot}}$ and $\epsilon_{\text{dc-VB}}$ suggest that two factors participate in determining the $\epsilon_{\text{dc-tot}}$ and $\epsilon_{\text{dc-VB}}$ values. One is the CT from [Cu(111) – nCu]^S to Ni, Pd, and Pt atoms, as discussed above. The other is the presence of the *d*-PDOS of Ni, Pd, and Pt at a higher energy than that of Cu, as shown in Figure 3 (d) ~ (f); the *d*-DOSs of nPd/Cu(111) are shown in Figures S11 ~ S14 of the SI. Particularly, the *d*-DOS of Ni exists at a much higher energy than that of Cu(111). In nNi/Cu(111)^S, therefore, the Ni *d*-DOS contributes to rising the $\epsilon_{\text{dc-tot}}$ and $\epsilon_{\text{dc-VB}}$ in energy, as going from Cu(111) to 4Ni/Cu(111)^S. In this alloy, the influence by the CT is small because the CT between the Ni_n cluster and the Cu(111) host is marginal (Figure 2). In the nPt/Cu(111) case, the CT largely occurs (Figure 2). Consequently, the $\epsilon_{\text{dc-tot}}$ and $\epsilon_{\text{dc-VB}}$ lower in energy as going from Cu(111) to 3Pt/Cu(111), because the CT from Cu(111) to Pt atoms contributes to lowering the $\epsilon_{\text{dc-tot}}$ and $\epsilon_{\text{dc-VB}}$ in energy. Then, they rise in energy when going from 3Pt/Cu(111) to 4Pt/Cu(111), because the contribution of the high energy Pt *d*-DOS becomes large in 4Pt/Cu(111)^S, as shown in Figure 3(f). In nPd/Cu(111), the CT is not very large compared to nPt/Cu(111), and therefore, only the presence of the high energy Pd 4*d* PDOS contributes to rising the $\epsilon_{\text{dc-tot}}$ and $\epsilon_{\text{dc-VB}}$ in energy, leading to the monotonous rise of the $\epsilon_{\text{dc-tot}}$ and $\epsilon_{\text{dc-VB}}$ in energy. However, the ϵ_{F} value monotonously lowers in energy in all nX/Cu(111) unlike in nX/Ni(111) when going from n = 0 to n = 4, which is not consistent with the complex energy

shifts of the $\varepsilon_{\text{dc-tot}}$ and $\varepsilon_{\text{dc-VB}}$. This seeming inconsistency is explained reasonably, as follows: The Cu atom has d and s electrons around the Fermi level but their DOSs are not large around the Fermi level. Because the CT mainly occurs from the high energy valence band around the Fermi level, the CT considerably influences the ε_{F} value in the $n\text{X}/\text{Cu}(111)$ case, even though it is marginal.

In conclusion, the ε_{F} , $\varepsilon_{\text{dc-tot}}$, and $\varepsilon_{\text{dc-VB}}$ of $n\text{X}^1/\text{Ni}(111)$ and $n\text{X}^2/\text{Cu}(111)$ differ from those of $\text{Ni}(111)$ and $\text{Cu}(111)$. The differences in $\varepsilon_{\text{dc-tot}}$ and $\varepsilon_{\text{dc-VB}}$ are larger than that in the ε_{F} . The energy shifts of $\varepsilon_{\text{dc-tot}}$ and $\varepsilon_{\text{dc-VB}}$ are induced by the CTs between $[\text{M}(111) - n\text{M}]_{\text{def}}^{\text{S}}$ and $n\text{X}$ atoms and between $[\text{M}(111) - \text{M}_n]_{\text{def}}^{\text{P}}$ and X_n cluster, and also by the presence of d bands of the X atom and X_n cluster. These changes in the ε_{F} , $\varepsilon_{\text{dc-tot}}$, and $\varepsilon_{\text{dc-VB}}$ suggest that the electronic structures of the $\text{Ni}(111)$ and $\text{Cu}(111)$ surfaces are controlled by alloy formation, which is discussed in the section 3.7.

3.6. Determination factor for E_{int}

Because the E_{int} term plays a key role in determining the relative stabilities of the SAA and PSA, as discussed in the section 3.4, it is important to elucidate the reason(s) why the E_{int} stabilizes the SAA compared to the PSA when going from $\text{X}^1 = \text{Cu}$ to $\text{X}^1 = \text{Au}$ in $n\text{X}^1/\text{Ni}(111)$ and from $\text{X}^2 = \text{Ni}$ to $\text{X}^2 = \text{Pt}$ in $n\text{X}^2/\text{Cu}(111)$, as shown in Tables 2 and 3. The Cu atom has a moderately positive charge, the Ag atom has a moderately negative charge, but the Au atom has a considerably negative charge in both SAA and PSA of $n\text{X}/\text{Ni}(111)$, as discussed above and shown in Figure 2. Therefore, it is likely that the valence orbitals of the Cu atom and the Cu_n cluster exist at a slightly higher energy than those of $[\text{Ni}(111) - n\text{Ni}]_{\text{def}}^{\text{S}}$ and $[\text{Ni}(111) - \text{Ni}_n]_{\text{def}}^{\text{P}}$, whereas those of the Ag atom and the Ag_n cluster exist at a moderately lower energy and those of the Au atom and Au_n cluster exist at a considerably lower energy than those of $[\text{Ni}(111) - n\text{Ni}]_{\text{def}}^{\text{S}}$ and $[\text{Ni}(111) - \text{Ni}_n]_{\text{def}}^{\text{P}}$.

Although the valence orbitals of Cu, Ag, and Au atoms are obviously 4s, 5s, and 6s orbitals, respectively, it is not clear what valence orbitals Cu_n, Ag_n, and Au_n clusters have. We inspected spin density of each atom of nX/Ni(111)^S and nX/Ni(111)^P. In both SAA and PSA, each Ni atom has considerable spin density around 0.60 *e* to 0.70 *e*. The Ni atoms interacting with the X atom or X_n cluster have moderately smaller spin density than the other Ni atoms interacting with neither X atom nor X_n cluster; details are shown in Table S9 of the SI. Although free Cu, Ag, and Au atoms have one spin on each atom, a negligibly small spin density is found on these atoms in nX/Ni(111)^S and nX/Ni(111)^P (Table S9). These features strongly suggest that the bonding interactions between one X atom and [Ni(111) – nNi]_{def}^S and between X_n cluster and [Ni(111) – Ni_n]_{def}^P are formed through spin-pairing using unpaired electrons of the X atom and X_n cluster. On the basis of this suggestion, it is likely that frontier orbitals of the X_n cluster with a high spin state play a role of valence orbital.

When the bonding interaction is formed between two species bearing different spins through spin pairing, the stabilization energy $\Delta E(A-B)$ is represented by eq. (11) on the basis of the simple Hückel MO theory.⁵⁹⁻⁶⁷

$$\Delta E(A - B) = \sqrt{(\epsilon_A - \epsilon_B)^2 + 4\beta^2} \quad (11)$$

where ϵ_A and ϵ_B are valence orbital energies of A and B, respectively, and β is a resonance integral between valence orbitals of A and B. This equation indicates that $\Delta E(A-B)$ becomes large as the $(\epsilon_A - \epsilon_B)$ term increases when β does not differ very much. This understanding has been applied to metal-particles, too;⁶⁸⁻⁷¹ the explanation is presented in page S31 of the SI. Although the metal system differs from the molecular system, the use of eq. (11) is not unreasonable because the metal system has a huge number of orbitals delocalized on whole system and the energy stabilization by one orbital is determined by eq. (11). Also, the CT occurs between the host and guest metals, which induces stabilization energy. The eq. (11) is

obtained by interaction between two orbitals bearing different orbital energies, indicating that the stabilization by CT is approximately represented by the eq. (11).

As discussed above, the valence orbitals of $[\text{Ni}(111) - n\text{Ni}]_{\text{def}}^{\text{S}}$ and $[\text{Ni}(111) - \text{Ni}_n]_{\text{def}}^{\text{P}}$ exist at a slightly lower energy than those of the Cu atom and Cu_n cluster. As going from one Cu atom to Cu_4 cluster, the α -HOMO energy considerably rises by 1.71 eV but the β -HOMO energy moderately lowers by 0.35 eV, as shown in Figure 4, where valence orbitals of Cu_2 and Cu_3 clusters are shown in Figure S15 of the SI; we need here to mention that the valence orbital energy changes in a similar manner upon going from one metal atom to metal cluster, from Ni to Pt, and from Cu to Au between the B3LYP and PBE functionals, as shown in Figures S16 and S17 of the SI. Because of these changes in orbital energy, the difference in valence orbital energy between the Cu_4 cluster and $[\text{Ni}(111) - \text{Ni}_4]_{\text{def}}^{\text{P}}$ is larger than that between one Cu atom and the $[\text{Ni}(111) - \text{Ni}]$. Therefore, the $E_{\text{int}}^{\text{P}}$ by the interaction between the Cu_4 cluster and $[\text{Ni}(111) - \text{Ni}_4]_{\text{def}}^{\text{P}}$ increases more than that by the interaction between 4 Cu atoms and $[\text{Ni}(111) - 4\text{Ni}]_{\text{def}}^{\text{S}}$. This is the reason why $4\text{Cu}/\text{Ni}(111)^{\text{P}}$ is more stable than $4\text{Cu}/\text{Ni}(111)^{\text{S}}$ and the energy difference between the PSA and SAA is larger in $4\text{Cu}/\text{Ni}(111)$ than in $2\text{Cu}/\text{Ni}(111)$.

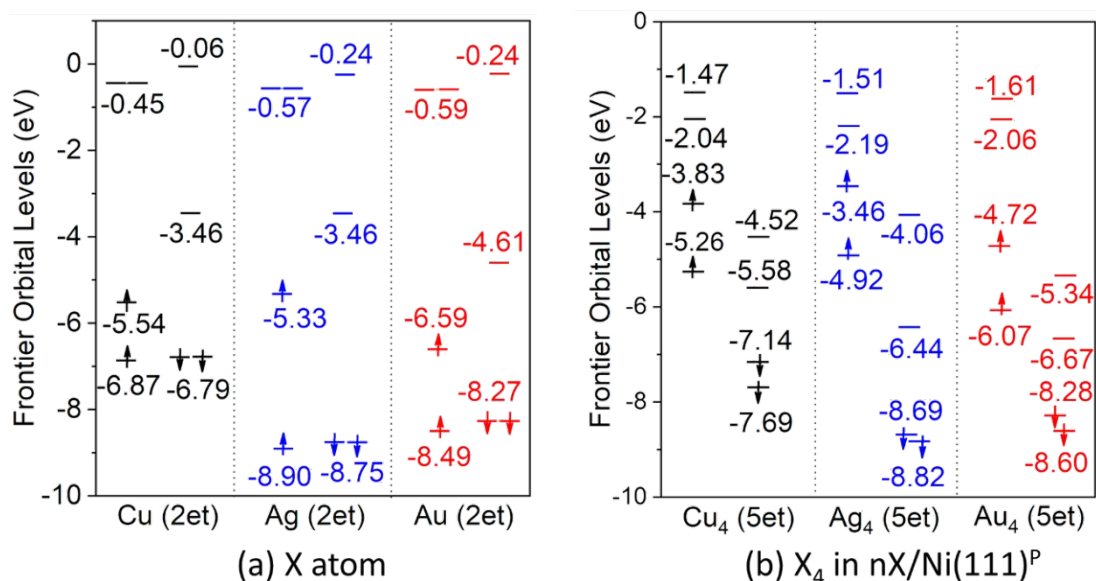


Figure 4. Energy levels of frontier orbitals of X atom and X_4 clusters, where the geometry of X_4 cluster was taken to be the same as that of $4X/\text{Ni}(111)^P$

The Ag atom has the α -HOMO at a slightly higher energy but the β -HOMO at a considerably lower energy than those of the Cu atom, strongly suggesting that a moderately negative charge of the Ag atom in $n\text{Ag}/\text{Ni}(111)$ results from the presence of its β -HOMO at a lower energy than that of the Cu atom. When going from one Ag atom to Ag_4 , the α -HOMO energy rises by 1.87 eV similarly to that of Cu_4 , whereas the β -HOMO energy changes little. Consequently, the E_{int}^P by the interaction between Ag_4 and $[\text{Ni}(111) - \text{Ni}_4]_{\text{def}}^P$ increases more than the E_{int}^S by the interaction between 4 Ag and $[\text{Ni}(111) - 4\text{Ni}]_{\text{def}}^S$, similarly to that of the Cu case, when going from one Ag to Ag_4 . Therefore, $4\text{Ag}/\text{Ni}(111)^P$ is more stable than $4\text{Ag}/\text{Ni}(111)^S$.

In the Au atom, both α -HOMO and β -HOMO exist at much lower energies than those of the Cu atom (Figure 4). Because of these features, the Au atom has a considerably negative charge in the $n\text{Au}/\text{Ni}(111)$. When going from one Au atom to Au_4 cluster, the α -HOMO energy considerably rises by 1.87 eV, whereas the β -HOMO energy changes little. Because the α -HOMO energy of one Au atom exists at a much lower energy than that of $[\text{Ni}(111) - n\text{Ni}]_{\text{def}}^S$, the considerable rise in the α -HOMO energy of the Au_4 cluster leads to the decrease in the $\varepsilon_A - \varepsilon_B$ term by the valence orbitals of Au_4 and $[\text{Ni}(111) - \text{Ni}_4]^P$. The E_{int}^P and E_{int}^S terms increase when going from $\text{Au}/\text{Ni}(111)$ to $4\text{Au}/\text{M}(111)$ because the number of interaction sites increases. However, the decrease in the $\varepsilon_A - \varepsilon_B$ term suppresses the increase in E_{int}^P when going from $\text{Au}/\text{Ni}(111)$ to $4\text{Au}/\text{Ni}(111)^P$. Therefore, the E_{int}^P value by the interaction between the Au_4 cluster and $[\text{Ni}(111) - \text{Ni}_4]_{\text{def}}^P$ increases less than that between 4 Au atoms and $[\text{Ni}(111) - n\text{Ni}]_{\text{def}}^S$, when going from $\text{Au}/\text{Ni}(111)$ to $4\text{Au}/\text{Ni}(111)$. Consequently, $4\text{Au}/\text{Ni}(111)^P$ is less stable than $4\text{Au}/\text{Ni}(111)^S$.

In $nX/Cu(111)$, the similar discussion is possible. The Cu and X atoms have nearly no spin density in Cu(111) and all the $nX/Cu(111)$ alloys studied here, as shown in Table S9 of the SI. This is consistent with the non-spin-polarized DOS of Cu(111) and $nX/Cu(111)$. Because the Cu atom has one unpaired electron, these features strongly suggest that spin pairing occurs among Cu and X atoms and X_n cluster in $nX/Cu(111)^P$. Therefore, it is likely that frontier orbitals of the X_n cluster with a high spin state play a role of valence orbital like in the case of $nX^I/Ni(111)$. In Ni/Cu(111), the Ni atomic charge is slightly negative, indicating that the valence orbital of the Ni atom exists at a slightly lower energy than that of [Cu(111) – Cu]. The Pd atom has the α -HOMO at a similar energy to but the β -HOMO at a much lower energy than those of the Ni atom, as shown in Figure 5. The lower energy β -HOMO leads to the presence of the moderately negative charge of the Pd atom in $nPd/Cu(111)$. The Pt atom has the α - and β -HOMOs at much lower energies than those of the Ni atom. Consequently, the Pt atom has a considerably negative charge.

When going from one Ni atom to the Ni_4 cluster, the α -HOMO energy considerably rises by 1.78 eV but the β -HOMO energy marginally rises (Figure 5). Because the α -HOMO of one Ni atom exists at a slightly lower energy than the valence orbital of [Cu(111) – Cu], the considerable rise in the α -HOMO energy increases the $\varepsilon_A - \varepsilon_B$ term by the Ni_4 cluster and [Cu(111) – Cu_4] $_{def}^P$. Consequently, the E_{int}^P by the interaction between Ni_4 and [Cu(111) – Cu_4] $_{def}^P$ increases more than the E_{int}^S by the interaction between 4 Ni atoms and [Cu(111) – $4Cu$] $_{def}^S$ when going from Ni/Cu(111) to $4Ni/Cu(111)$. Therefore, $4Ni/Cu(111)^P$ becomes more stable than $4Ni/Cu(111)^S$.

The α -HOMO of the Pd atom exists at a similar energy to but the β -HOMO exists at a considerably lower energy than those of the Ni atom (Figure 5). This feature means that the $\varepsilon_A - \varepsilon_B$ term by the β -HOMO and the valence orbital of [Cu(111) – Cu] is larger in the Pd case than in the Ni case. When going from one Pd atom to the Pd_4 cluster, the α -HOMO energy

rises in energy like that of the Ni case but the β -HOMO energy changes marginally. Because the α - and β -HOMO energies of the Pd case change similarly to those of the Ni case, the $E_{\text{int}}^{\text{P}}$ increases similarly to that of the Ni case, when going from one Pd atom to the Pd₄ cluster. However, the β -HOMO energy of one Pd atom is considerably lower than that of one Ni atom, leading to the presence of the larger $\varepsilon_{\text{A}} - \varepsilon_{\text{B}}$ term for one Pd atom and [Cu(111) – Cu] than that of the Ni case and therefore, nPd/Cu(111) tends to form SAA compared to nNi/Cu(111). Because nNi/Cu(111)^S is as stable as nNi/Cu(111)^P, as seen in Table 1, the SAA becomes more stable than the PSA in nPd/Cu(111). Here, we need to mention that the $E_{\text{int}}^{\text{S}}$ of nPd/Cu(111) is smaller than that of nNi/Cu(111) in Tables 2 and 3, which is seemingly inconsistent with the discussion above. However, the conclusion that the nPd/Cu(111) tends to have SAA compared to nNi/Cu(111) is reasonable, as follows: Because the Pd position deviates from the best for orbital interaction with Cu(111), both $E_{\text{int}}^{\text{P}}$ and $E_{\text{int}}^{\text{S}}$ of nPd/Cu(111) decrease compared to those of nNi/Cu(111), as discussed below in more detail. This is the reason why the $E_{\text{int}}^{\text{S}}$ of nPd/Cu(111) is smaller than that of nNi/Cu(111). However, the $\varepsilon_{\text{A}} - \varepsilon_{\text{B}}$ term is favorable for presenting the larger $E_{\text{int}}^{\text{S}}$ value between four Pd and [Cu(111) – 4Cu]^S than the $E_{\text{int}}^{\text{P}}$ value between Pd₄ and [Cu(111) – Cu₄]^P. As a result, nPd/Cu(111)^S is more stable than nPd/Cu(111)^P.

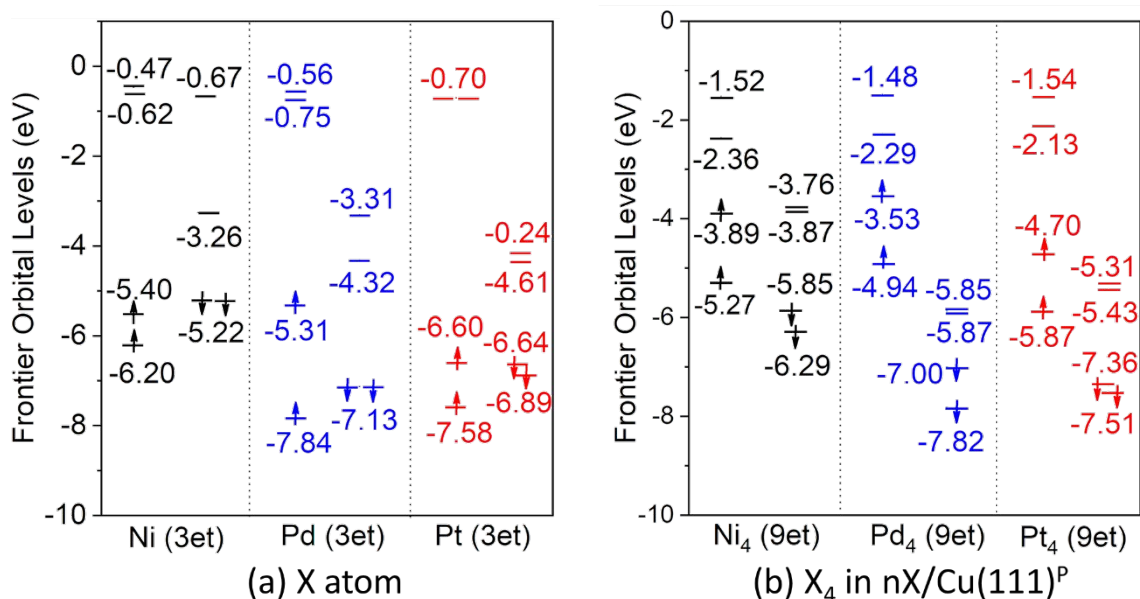


Figure 5. Energy levels of frontier orbitals of the X atom and X₄ clusters, where the geometry of X₄ cluster was taken to be the same as that of 4X/Cu(111)^P

When going from one Pt atom to Pt₄ cluster, the α -HOMO considerably rises in energy by 1.90 eV, whereas the β -HOMO somewhat lowers in energy by 0.72 eV. Because the β -HOMO of one Pt atom exists at a lower energy than that of [Cu(111) – Cu], the $\varepsilon_A - \varepsilon_B$ term by the β -valence orbitals of the Pt₄ cluster and [Cu(111) – Cu₄]_{def}^P is larger than that by one Pt atom and [Cu(111) – Cu]. Therefore, the E_{int}^P by the β -HOMO increases when going from one Pt atom to the Pt₄ cluster. However, the rise of the α -HOMO energy of the Pt₄ cluster decreases the $\varepsilon_A - \varepsilon_B$ term by the α -HOMO of the Pt₄ and the valence orbital of [Cu(111) – Cu₄]_{def}^P, because the α -HOMO of one Pt atom exists at a lower energy than that of [Cu(111) – Cu]. Because the α -HOMO energy changes more than the β -HOMO energy, the E_{int}^P by the α -HOMO decreases more than the E_{int}^P by the β -HOMO increases. When going from one Pt atom to the Pt₄ cluster, both E_{int}^P and E_{int}^S terms increase because the Pt₄ cluster and 4 Pt atoms have more interaction sites than one Pt atom, as discussed above. However, the $\varepsilon_A - \varepsilon_B$ term suppresses the increase in E_{int}^P , because the $\varepsilon_A - \varepsilon_B$ term by the α -HOMO decreases when going from one Pt atom to Pt₄ cluster to decrease the E_{int}^P value more than the $\varepsilon_A - \varepsilon_B$

term by the β -HOMO increases the $E_{\text{int}}^{\text{P}}$. Therefore, the $E_{\text{int}}^{\text{P}}$ value by the interaction between the Pt_4 cluster and $[\text{Cu}(111) - \text{Cu}_4]_{\text{def}}^{\text{P}}$ increases less than that between 4 Pt atoms and $[\text{Cu}(111) - 4\text{Cu}]_{\text{def}}^{\text{S}}$ when going from one Pt atom to 4 Pt atoms. As a result, $4\text{Pt}/\text{Cu}(111)^{\text{P}}$ is less stable than $4\text{Pt}/\text{Cu}(111)^{\text{S}}$.

Here, we have to notice that both $E_{\text{int}}^{\text{S}}$ value by the interactions between n X atoms and $[\text{Ni}(111) - n\text{Ni}]_{\text{def}}^{\text{S}}$ and $E_{\text{int}}^{\text{P}}$ value by the interactions between X_n cluster and $[\text{Ni}(111) - \text{Ni}_n]_{\text{def}}^{\text{P}}$ decrease when going from $\text{X} = \text{Cu}$ to $\text{X} = \text{Au}$, as shown in Tables 2 and 3. Similarly, both $E_{\text{int}}^{\text{S}}$ value by the interactions between n Pd atoms and $[\text{Cu}(111) - n\text{Cu}]_{\text{def}}^{\text{S}}$ and $E_{\text{int}}^{\text{P}}$ value by the interactions between Pd_n and $[\text{Cu}(111) - \text{Cu}_n]_{\text{def}}^{\text{P}}$ are smaller than those of the Ni cases. However, the above discussion based on eq. (11) suggests that they increase. This discrepancy between the change in E_{int} and the above discussion based on eq. (11) may arise from the atomic sizes of these elements; the atomic radius is 1.25 Å for Ni, 1.28 Å for Cu and 1.44 Å for Ag and Au. Because the atomic radius of Ni is similar to that of Cu, the Ni–Cu distance in $n\text{Cu}/\text{Ni}(111)$ is close to the Ni–Ni distance of Ni(111), which does not cause largely the distortion of the Ni(111) moiety by Ni–Cu exchange. However, the Ni–Ag and Ni–Au distances in $n\text{Ag}/\text{Ni}(111)$ and $n\text{Au}/\text{Ni}(111)$ are considerably longer than the Ni–Ni distance, as discussed above and seen in Figure 1, because of the larger atomic radii of Ag and Au than that of Ni. This means that the Ag and Au atoms cannot take a good position for the orbital interaction in $n\text{Ag}/\text{Ni}(111)$ and $n\text{Au}/\text{Ni}(111)$. Indeed, the Ag and Au atoms exist at higher positions than the surface Cu atom in $n\text{X}/\text{Cu}(111)$ alloys, as discussed above. In other words, the Ag and Au atoms take the deviated position from the best one for bonding interacting with the surface Cu atom, which reduces the orbital overlap and sacrifices the stabilization energy. This is the reason why the E_{int} value decreases when going from $n\text{Cu}/\text{Ni}(111)$ to $n\text{Ag}/\text{Ni}(111)$ and $n\text{Au}/\text{Ni}(111)$. The same explanation is possible for

nNi/Cu(111) and nPd/Cu(111) because the atomic radius of Ni is similar to but that of Pd is considerably larger than that of Cu.

The atomic radius influences similarly both $E_{\text{int}}^{\text{S}}$ and $E_{\text{int}}^{\text{P}}$ values because the position deviation does not differ very much between n X atoms and X_4 cluster. Therefore, it is true that when going from nCu/Ni(111) to nAu/Ni(111) $E_{\text{int}}^{\text{S}}$ and $E_{\text{int}}^{\text{P}}$ values decrease and that when going from one Au atom to the Au_4 cluster and from one Pd atom to the Pd_4 cluster the valence orbital of X_n rises in energy to reduce the stabilization energy by the $E_{\text{int}}^{\text{P}}$ term compared to the $E_{\text{int}}^{\text{S}}$ value. It is concluded that the energy level of valence orbital of the X_n cluster is an important determination factor for relative stabilities of SAA and PSA.

Because SAA bearing guest metal(s) on the surface is desirable for catalyst, we will discuss here what factor(s) is important for producing such a structure, summarizing the above results and referring the review by Johnston and coworkers.⁷² Atomic radii of guest atom and host atoms and CT between the host and the guest are considered to be plausible determination factors of alloy structure, as follows: Ni atom penetrates into Cu(111) but Pd and Pt atoms do not, as discussed above (the section of “Models”). Also, Cu, Ag, and Au atoms do not penetrate into Ni(111). The atomic radius of the Ni atom is moderately smaller than that of the Cu atom, which facilitates the penetration of Ni into Cu(111). However, the Cu atom does not penetrate into Ni(111). This is reasonable because the Cu atom is moderately larger than the Ni atom. Because the Ag and Au atoms are considerably larger than the Ni atom and the Pd and Pt atoms are considerably larger than the Cu atom, the Ag and Au atoms do not penetrate into Ni(111) and the Pd and Pt do not into Cu(111). Thus, the atomic radius is one of important factors for stabilizing the SAA structure bearing guest metal atom on the surface. Valence orbital energy of metal atom is another important factor for determining whether atomically dispersed distribution is stable or not, as summarized below: When the valence orbital of host metal atom exists at a higher energy than that of guest metal atom, the bonding

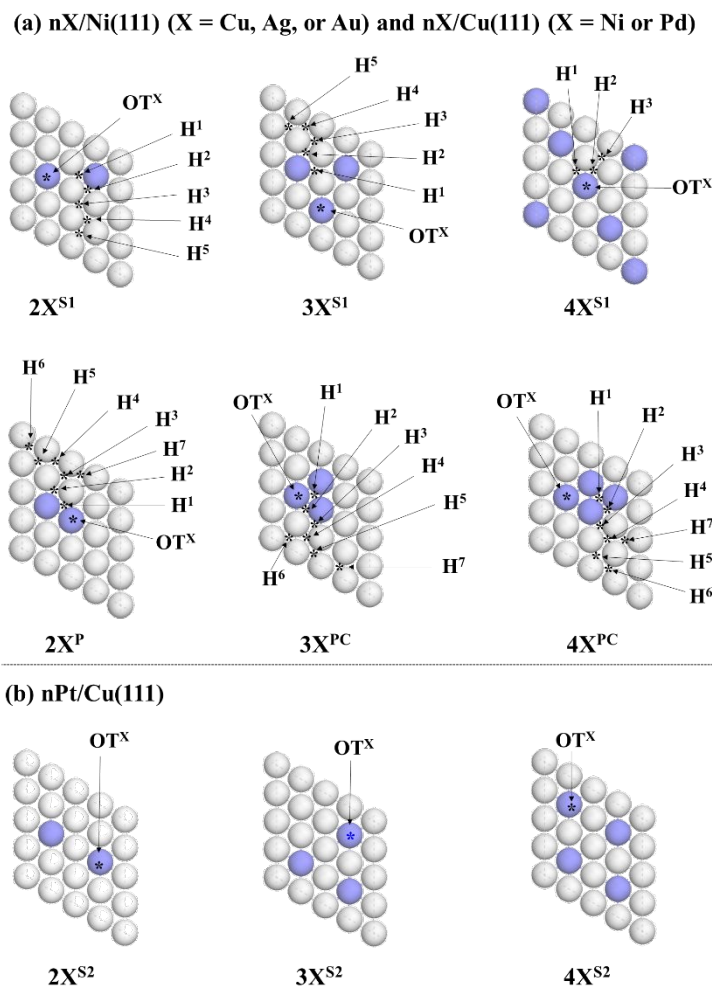
interaction between the cluster of guest metal atoms and the host is weaker than that between one guest metal atom and the host because the valence orbital of metal cluster rises in energy to decrease the $\varepsilon_A - \varepsilon_B$ term in eq. (11). This means that the use of guest metal atom bearing valence orbital at lower energy than that of host metal atom is recommended for producing SAA. Considering these two factors, one guideline on producing SAA bearing guest metal(s) at the surface is to use guest metal atom(s) with a larger atomic radius and valence orbital at lower energy than those of host metal atom.

3.7. CO adsorption to $nX^1/\text{Ni}(111)$ ($X^1 = \text{Cu, Ag, or Au}$) and $nX^2/\text{Cu}(111)$ ($X^2 = \text{Ni, Pd, or Pt}$)

The surface reactivity of these alloys is explored taking CO adsorption as one example, because CO adsorption is often investigated to evaluate reactivity of metal surface. We investigated all plausible adsorption sites, as shown in Scheme 3 and listed CO adsorption energy (E_{ads}) at the most stable site in Table 5; those of the less stable CO adsorptions to the Ni(111), Cu(111), $nX/\text{Ni}(111)$, and $nX/\text{Cu}(111)$ surfaces are presented in Tables S10 ~ S12 of the SI.

On the pure Ni(111) surface, the E_{ads} value is -1.92 eV, -1.79 eV, and -1.56 eV at the hollow (**H**), bridge (**B**), and on-top (**OT**) sites, respectively, as shown in Table S10 of the SI. On the pure Cu(111) surface, the E_{ads} value is -0.95 eV, -0.87 eV, and -0.78 eV at the **H**, **B**, and **OT** sites, respectively. These results show that the CO adsorption at the **H** site is the most stable in both Ni(111) and Cu(111) surfaces and that the CO adsorption to the Ni(111) surface occurs much more strongly than to the Cu(111) surface: The adsorption structure is essentially the same as that reported previously by theoretical works⁷³⁻⁷⁹ and these E_{ads} values at the **H** site are close to the previously calculated values, as shown in Table S13 of the SI. The

adsorbed CO is negatively charged by $-0.38 e$ and $-0.32 e$ at the **H** site on the Ni(111) and Cu(111) surfaces, respectively, showing that CT occurs from the metal surface to CO.



Scheme 3. Several important adsorption sites for CO on $nX/Ni(111)$ ($X = Cu, Ag, Au$) and $nX/Cu(111)$ ($X = Ni, Pd$) (a) and $nPt/Cu(111)$ (b)

In $2Cu/Ni(111)^P$, the CO adsorption does not occur at the **H** sites neighboring to the Cu atom(s) such as **H**² of $2X^{S1}$ and $2X^P$ but occurs at the **H**³ site surrounded by three Ni atoms with almost equal E_{ads} value to that of the Ni(111) surface, where **H**² and **H**³ etc. are shown in Scheme 3 and Table S11 of the SI. In $3Cu/Ni(111)^{PC}$ and $4Cu/Ni(111)^{PC}$, the CO adsorption occurs at the **H**⁴ site, which corresponds to the **H**³ site of $2Cu/Ni(111)^P$. This is reasonable because CT occurs to the Ni atom from the Cu atom and because the Cu atoms are close to the

Ni atoms surrounding the \mathbf{H}^3 site of $2\text{Cu}/\text{Ni}(111)^{\text{P}}$ and the \mathbf{H}^4 site of $3\text{Cu}/\text{Ni}(111)^{\text{P}}$, as shown in Figure 3. Indeed, the charge of the Ni atoms in $n\text{Ni}/\text{Cu}(111)$ is slightly more negative than that in $\text{Ni}(111)$, as shown in Table 5, which is favorable for the CT to the CO molecule. In $2\text{Ag}/\text{Ni}(111)^{\text{S1}}$, $3\text{Ag}/\text{Ni}(111)^{\text{PC}}$, $4\text{Ag}/\text{Ni}(111)^{\text{PC}}$, and $n\text{Au}/\text{Ni}(111)^{\text{S1}}$, CO adsorption occurs at the \mathbf{H}^5 site distant from Ag and Au atoms. It is noteworthy that the E_{ads} value is slightly larger in $n\text{Cu}/\text{Ni}(111)$ than in $\text{Ni}(111)$ but smaller in $n\text{Ag}/\text{Ni}(111)$ and considerably smaller in $4\text{Au}/\text{Ni}(111)^{\text{S1}}$ than in $4\text{Cu}/\text{Ni}(111)^{\text{PC}}$. These results are consistent with the facts showing that CT occurs moderately from Cu_n cluster to Ni atoms in $n\text{Cu}/\text{Ni}(111)$, moderately from Ni atoms to $n\text{Ag}$ atoms in $n\text{Ag}/\text{Ni}(111)$, and considerably from Ni atoms to $n\text{Au}$ atoms in $n\text{Au}/\text{Ni}(111)$. Because the CT occurs from the $\text{Ni}(111)$ host to n Ag and n Au atoms, the Ni atoms on the surface are electron-deficient in $4\text{Ag}/\text{Ni}(111)$ and $4\text{Au}/\text{Ni}(111)$ than in $\text{Ni}(111)$, as shown in Table 5, and the $\epsilon_{\text{dc-VB}}$ energy is lower in $4\text{Ag}/\text{Ni}(111)^{\text{S1}}$ and $4\text{Au}/\text{Ni}(111)^{\text{S1}}$ than in $4\text{Cu}/\text{Ni}(111)^{\text{PC}}$ (Table 4). Consequently, the CT from $4\text{Ag}/\text{Ni}(111)^{\text{S1}}$ and $4\text{Au}/\text{Ni}(111)^{\text{S1}}$ to CO occurs more weakly than those from the $\text{Ni}(111)$ and $n\text{Cu}/\text{Ni}(111)^{\text{P}}$. This is the reason of the smaller E_{ads} in $4\text{Ag}/\text{Ni}(111)^{\text{S1}}$ and $4\text{Au}/\text{Ni}(111)^{\text{S1}}$ than in $n\text{Cu}/\text{Ni}(111)^{\text{P}}$. To compare the CO adsorption between $\text{Ni}(111)$ and $n\text{Au}/\text{Ni}(111)$ in more detail, we calculated C-O stretching frequency (ν_{CO}) and found that the ν_{CO} value of CO adsorbed on $4\text{Au}/\text{Ni}(111)^{\text{S}}$ is lower than that on $\text{Ni}(111)$ by 16 cm^{-1} . This lower frequency shift agrees well with the experimental result,^{80, 81} as shown in Table S13 of the SI. Though the calculated frequency (1759 cm^{-1}) of ν_{CO} in the $\text{Ni}(111)$ case is somewhat lower than the experimental value (1816 cm^{-1}), the difference is not very unreasonable because the ν_{CO} value depends on the CO coverage; actually, only one CO molecule is adsorbed in the present model for calculation but it is not clear how many CO molecules are adsorbed at the surface in experiment. In $\text{Cu}(111)$, the calculated ν_{CO} value is close to the experimental one (Table S13).⁸²

Table 5. The CO adsorption energy (E_{ads} in eV) in the most stable CO adsorption structure, the Bader charge of the adsorbed CO (Q_{CO} in e), and the Bader charge of the M (or X) atoms before the CO adsorption (Q_{M} (or Q_{X}) in e).

nX/Ni(111) (X = Cu, Ag, or Au)				nX/Cu(111) (X = Ni, Pd, or Pt)			
Models	$E_{\text{ads}}(\text{site})^{\text{a}}$	Q_{CO}	Q_{M}	Models	$E_{\text{ads}}(\text{site})^{\text{a}}$	Q_{CO}	Q_{X}^{b}
Ni(111)	-1.92 (H)	-0.38	-0.08	Cu(111)	-0.95 (H)	-0.38	-0.08
2Cu ^P	-1.93 (H ³)	-0.38	-0.08	2Ni ^{S1}	-1.70 (OT ^X) ^c	-0.26	-0.09
3Cu ^{PC}	-1.95 (H ⁴)	-0.38	-0.09	3Ni ^{S1}	-1.69 (OT ^X)	-0.09	-0.10
4Cu ^{PC}	-1.94 (H ⁴)	-0.38	-0.09	4Ni ^{PC}	-2.14 (H ¹)	-0.38	-0.24
2Ag ^{S1}	-1.86 (H ⁵)	-0.37	-0.08	2Pd ^{S1}	-1.15 (OT ^X)	-0.11	-0.36
3Ag ^{PC}	-1.86 (H ⁵)	-0.37	-0.03	3Pd ^{S1}	-1.14 (OT ^X)	-0.12	-0.36
4Ag ^{PC}	-1.82 (H ⁵)	-0.36	-0.04	4Pd ^{S1}	-1.13 (OT ^X)	-0.13	-0.36
2Au ^{S1}	-1.88 (H ⁵)	-0.35	-0.07	2Pt ^{S2}	-1.51 (OT ^X)	-0.10	-0.64
3Au ^{S1}	-1.86 (H ⁵)	-0.34	0.09	3Pt ^{S2}	-1.50 (OT ^X)	-0.10	-0.64
4Au ^{S1}	-1.70 (H ³)	-0.35	0.03	4Pt ^{S2}	-1.48 (OT ^X)	-0.10	-0.65

a) The positions H³, H⁴, etc. are shown in Scheme 3. b) The superscript X represents that the CO adsorption occurs at the X atom. c) The E_{ads} is -2.03 eV for the CO adsorption at the H site of Pd(111) and -1.88 eV for that of Pt(111).

In nX²/Cu(111) (X² = Ni, Pd, or Pt), CO is adsorbed more strongly with the X² atom than with the Cu atom, as shown in Table 5 and Table S12 of the SI. This feature is understood in terms of the d -valence band energy, as follows: CO tends to bind with the metal atom bearing the occupied d orbital at a high energy to form a strong CT from the metal to the CO molecule. As shown in Figures 3 (d) to (f) and Figures S11 ~ S14 of the SI, the d -valence bands of Ni, Pd, and Pt exist at a much higher energy than that of Cu(111). Consequently, CO adsorption occurs at the Pd and Pt atoms in the on-top manner except for 4Ni/Cu(111)^{PC} in which the CO adsorption occurs at the hollow site surrounded by three Ni atoms. The E_{ads} is much larger in nNi/Cu(111) than in nPd/Cu(111)^S and nPt/Cu(111)^S. This is attributable to the presence of the d -DOS at a high energy in nNi/Cu(111), too, because the valence band d -DOS of Ni exists

at a higher energy than those of Pd and Pt, as shown in Figures 3 (e) and (f) and Figures S11 ~ S14 of the SI. In 4Ni/Cu(111)^{PC}, the CO adsorption occurs at the **H**¹ site surrounded by three Ni atoms like that on the Ni(111) surface but the E_{ads} value is considerably larger than those at the other sites in 4Ni/Cu(111)^{PC}. The E_{ads} value is even larger than that of the pure Ni(111) (Table 5). This large E_{ads} value is reasonable, because the Ni atom is negatively charged in 4Ni/Cu(111)^{PC} due to the CT from Cu(111) to Ni atoms.

On the other hand, the CO adsorption occurs to nPd/Cu(111)^S and nPt/Cu(111)^S with considerably smaller E_{ads} values than those to the pure Pd (111) and Pt(111) surfaces ($E_{\text{ads}} = -2.03$ eV and -1.88 eV, respectively). This result is against the expectation from the fact showing that the Pd and Pt atoms are negatively charged in these alloys due to the CT from the Cu(111) to Pd and Pt atoms. The considerably small E_{ads} value does not result from the negatively charged Pd and Pt atoms but from the difference in the CO adsorption structure; in the pure Pd(111) and Pt(111) surfaces, the CO adsorption occurs at the **H** site like that on the Ni surface, whereas the CO adsorption occurs at the on-top (**OT**) site in nPd/Cu(111)^S and nPt/Cu(111)^S. These results suggest that the reactivity toward CO is enhanced in nNi/Cu(111)^{PC} but weakened in nPd/Cu(111)^S and nPt/Cu(111)^S. This is important finding because the CO poisoning is suppressed using Cu-based SAAs of Pd and Pt.

4. CONCLUSIONS

In this work, we carried out a theoretical study of SAA and PSA of nX/M(111) ($X^1 = \text{Cu}$, Ag, or Au for $M = \text{Ni}$; $X^2 = \text{Ni}$, Pd, or Pt for $M = \text{Cu}$; $n = 1 \sim 4$). DFT calculations disclosed that PSA is more stable than SAA in nCu/Ni(111) but SAA is more stable than PSA in nAu/Ni(111), nPd/Cu(111), and nPt/Cu(111). In the nAg/Ni(111) and nNi/Cu(111), relative stabilities of SAA and PSA depend on the coverage of Ag on Ni(111) and that of Ni on Cu(111). These results agree with the experimental observations.^{4,10,19-21,26,27,29-31}

To obtain better understanding, we analyzed energy changes along assumed reaction to generate SAA and PSA of $nX/M(111)$ from $M(111)$ and $n X$ atoms. This analysis elucidated that the interaction energy E_{int} of $M(111)$ with either $n X$ atoms or X_n cluster plays an important role in determining which of SAA and PSA is produced. In Ni- and Cu-based alloys, the Ni(111) and Cu(111) hosts have their $3d$ valence orbitals at a higher energy than those of $5d$ metal elements such as Au and Pt. Because the valence orbitals of Au_4 cluster exist at higher energies than those of Au atom, the $\varepsilon_A - \varepsilon_B$ term by valence orbitals of the Au_n cluster and Ni(111) host is smaller than that by one Au atom and the Ni(111) host. The E_{int} increases (gets more negative) when going from $Au/Ni(111)$ to $4Au/Ni(111)^P$, because the X_4 cluster has more interaction sites than one X atom. However, the decrease in the $\varepsilon_A - \varepsilon_B$ term suppresses the increase in the E_{int}^P value by the interaction between Au_4 and the Ni(111) host compared to the E_{int}^S value between 4 Au atoms and the Ni(111) host. Therefore, the PSA becomes unstable compared to the SAA in $nAu/Ni(111)$. The same understanding is presented for $nPt/Cu(111)$. This result leads to a general prediction that the combination of $3d$ -base metal element M and $5d$ metal element X tends to provide the SAA of $nX/M(111)$ because the $5d$ orbital exists generally at a lower energy than the $3d$ orbital and the valence orbital rises in energy when going from one X atom to X_4 cluster. In $nCu/Ni(111)$, the Ni atom has a valence orbital at a slightly lower energy than that of Cu(111). The Cu_n cluster has a valence orbital at a considerably higher energy than the Cu atom to increase the E_{int}^P value between the Cu_n cluster and the Ni(111) host. Therefore, the PSA is more stable than the SAA in $nCu/Ni(111)$. The $4d$ metal elements exhibit intermediate behavior between $3d$ and $5d$ metal elements.

In $nX^1/Ni(111)$ ($X^1 = Cu, Ag, \text{ or } Au$), the Cu atom has a slightly positive atomic charge but the Ag and Au atoms have a negative atomic charge. In $nX^2/Cu(111)$ ($X^2 = Ni, Pd, \text{ or } Pt$), Ni, Pd, and Pt atoms have a negative atomic charge. These results indicate that the CT occurs between the $M(111)$ host and either X atom or X_n cluster. The CT influences the Fermi level

(ϵ_F), d -band center (ϵ_{dc-tot}), and d -valence band center (ϵ_{dc-vB}) of the alloy. In nCu/Ni(111) and nAg/Ni(111), the ϵ_F value does not differ very much from those of the pure Ni(111) surface because of the moderate CT, whereas it lowers considerably in nAu/Ni(111) because of the large CT. In nX²/Cu(111), the ϵ_F value lowers in energy compared to that of Cu(111). The ϵ_{dc-vB} value lowers considerably in nX¹/Ni(111) as n increases. In nNi/Cu(111), the ϵ_{dc-vB} value rises in energy as going from Cu(111) to nNi/Cu(111). In nPd/Cu(111) and nPt/Cu(111), however, the ϵ_{dc-vB} moderately lowers when going from $n = 0$ to $n = 2$ or 3 but then rises when going from $n = 2$ or 3 to $n = 4$. These complex changes are induced by two factors: one is the CT from Cu(111) to Pd and Pt atoms, which contributes to the energy lowering of the ϵ_{dc-vB} , and the other is the presence of the higher energy d -DOSs of Ni, Pd, and Pt atoms than that of Cu, which contributes to the energy rise of ϵ_{dc-vB} .

In nCu/Ni(111), CO adsorption occurs at the hollow site surrounded by Ni atoms neighboring to Cu atom, because CT moderately occurs from Ni(111) to Cu atoms. Because of the CT, CO adsorption energy is larger than that to the pure Ni(111). In nAg/Ni(111)^S and nAu/Ni(111)^S, CO adsorption occurs at the hollow site distant from Ag and Au atoms because CT occurs from the Ni(111) host to Ag and Au atoms. CO adsorption energy decreases as the number of Ag and Au atoms increases, because the CT from the Ni(111) host to Ag and Au atoms strengthens as the number of Ag and Au atoms increases. In nX/Cu(111)^S ($X = \text{Ni, Pd, or Pt}$), CO is adsorbed more strongly with the X atom than with the Cu(111) surface, because the X atom has a d -valence band at a higher energy than the Cu(111) host, which is favorable for the CT from the X atom to CO. However, the CO adsorption energy is smaller in the nPd/Cu(111)^S and nPt/Cu(111)^S than in Pd(111) and Pt(111), respectively, because the CO adsorption occurs at the hollow site of Pd(111) and Pt(111) but at the on-top site of the Pd atom in nPd/Cu(111)^S and on the Pt atom in nPt/Cu(111)^S. This feature strongly suggests that

the CO poisoning of Pd and Pt catalysts is suppressed by using Cu-based single-atom alloys of Pd and Pt.

This work clearly shows the general understanding why SAA is produced by the combinations of Au atoms with Ni(111) and Pd/Pt atoms with Cu(111) but PSA is produced by the combinations of Cu atoms with Ni(111) and Ni atoms with Cu(111). Also, important properties such as the Bader charge, ϵ_F , ϵ_{dc-tot} , and ϵ_{dc-VB} of the Ni- and Cu-based alloys presented here are valuable for understanding and predicting the reactivity of these alloys.

ASSOCIATED CONTENT

Supporting Information: 1. Effects of D3 correction on the CO adsorption and the relative energies of alloys (**Tables S1** and **S2**); 2. Geometries and relative stabilities of nX/M(111) alloy with X at the surface and the inside (**Scheme S1** and **Table S3**); 3. Various possible geometries and relative energies of SAA and PSA (**Figures S1 ~ S6**); 4. The geometries of the SAA and PSA explored in this work (**Scheme S2**); 5. Geometries of nX/M(111) employed in Tables 2, 3, S4, and S5 (**Scheme S3**); 6. Energy changes in SAA formation and PSA formation from M(111) and nX atoms (**Tables S4** and **S5**); 7. The Bader charge of nX atoms and X_n cluster, the Fermi level, d band center of nX/M(111) (**Tables S6 ~ S8**); 8. PDOSs of M(111) and nX/M(111) (**Figures S7 ~ S14**); 9. Spin density of M around X in nX/M(111): (**Table S9**); 10. A-B bond strength and valence orbital energies of A and B (**Scheme S4**); 11. Frontier orbitals of X_n clusters (**Figures S15 ~ S17**); 12. Adsorption sites, adsorption energy, and the Bader charge of CO adsorbed to the surfaces of M(111) and nX/M(111) (**Schemes S5** and **S6** and **Tables S10 ~ S12**); 13. The adsorption energy ($E_{ads(CO)}$ in eV) and C-O bond stretching vibration frequency ($\nu_{(C-O)}$ in cm^{-1}) of CO at the hollow site of Ni(111) and Cu(111) (**Table S13**); Fractional Coordinates.

AUTHOR INFORMATION

Corresponding Author

*E-mail: sakaki.shigeyoshi.47e@st.kyoto-u.ac.jp. Phone: +81-75-383-3036.

ORCID

Junqing Yin: 0000-0002-5240-4256

Masahiro Ehara: 0000-0002-2185-0077

Shigeyoshi Sakaki: 0000-0002-1783-3282

Notes

The authors declare no competing financial interest.

ACKNOWLEDGMENTS

We would like to thank Japan Science and Technology Agency (JST) for the partial financial support through CREST (Grant Number JPMJCR20B6) and Ministry of Education, Culture, Science, Sports and Technology (MEXT), Japan through the “Element Strategy Initiative for Catalysts and Batteries (ESICB)” (Grant Number JPMXP0112101003). We wish to thank the Electronic Computer Center of the National Institute for Physiological Sciences (Okazaki, Japan) for using super computers.

REFERENCES

-
- [1] S. Lee, L. Ji, A. C. D. Palma, and E. T. Yu, Scalable, highly stable Si-based metal-insulator-semiconductor photoanodes for water oxidation fabricated using thin-film reactions and electrodeposition. *Nat. Commun.* **2021**, *12*, 3982.
- [2] Y. J. Wang, N. Zhao, B. Fang, H. Li, X. T. Bi, and H. Wang, Carbon-supported Pt-based alloy electrocatalysts for the oxygen reduction reaction in polymer electrolyte membrane fuel cells: particle size, shape, and composition manipulation and their impact to activity. *Chem. Rev.* **2015**, *115*, 3433–3467.
- [3] B. Qiao, A. Wang, X. Yang, L. F. Allard, Z. Jiang, Y. Cui, J. Liu, J. Li, and T. Zhang, Single-atom catalysis of CO oxidation using Pt₁/FeO_x. *Nat. Chem.* **2011**, *3*, 634–641.

-
- [4] G. Sun, Z. J. Zhao, R. Mu, S. Zha, L. Li, S. Chen, K. Zang, L. Luo, Z. Li, S. C. Purdy, A. J. Kropf, J. T. Miller, L. Zeng, and J. Gong, Breaking the scaling relationship via thermally stable Pt/Cu single atom alloys for catalytic dehydrogenation. *Nat. Commun.* **2018**, *9*, 4454.
- [5] A. Wang and L. Olsson, The impact of automotive catalysis on the United Nations sustainable development goals. *Nat. Catal.* **2019**, *2*, 566–570.
- [6] I. E. L. Stephens, J. Rossmeisl, and I. Chorkendorff, Toward sustainable fuel cells. *Science* **2016**, *354*, 1378–1379.
- [7] T. Hirakawa, Y. Shimokawa, W. Tokuzumi, T. Sato, M. Tsushida, H. Yoshida, J. Ohyama, and M. Machida, Multicomponent 3d transition-metal nanoparticles as catalysts free of Pd, Pt, or Rh for automotive three-way catalytic converters. *ACS Appl. Nano Mater.* **2020**, *3*, 9097–9107.
- [8] S. De, J. Zhang, R. Luque, and N. Yan, Ni-based bimetallic heterogeneous catalysts for energy and environmental applications. *Energy Environ. Sci.* **2016**, *9*, 3314–3347.
- [9] B. Singh, V. Sharma, R. P. Gaikwad, P. Fornasiero, R. Zbořil, and M. B. Gawande, Single-atom catalysts: a sustainable pathway for the advanced catalytic applications. *Small.* **2021**, *17*, 2006473.
- [10] G. Kyriakou, M. B. Boucher, A. D. Jewell, E. A. Lewis, T. J. Lawton, A. E. Baber, H. L. Tierney, M. Flytzani-Stephanopoulos, and E. C. H. Sykes, Isolated metal atom geometries as a strategy for selective heterogeneous hydrogenations. *Science* **2012**, *335*, 1209–1212.
- [11] I. V. Yentekakis, P. Panagiotopoulou, and G. A. Artemakis, review of recent efforts to promote dry reforming of methane (DRM) to syngas production via bimetallic catalyst formulations. *Appl. Catal. B: Environ.* **2021**, *296*, 120210.
- [12] A. H. Dam, H. Wang, R. Dehghan-Niri, X. Yu, J. C. Walmsley, A. Holmen, J. Yang, and D. Chen. Methane activation on bimetallic catalysts: properties and functions of surface Ni–Ag alloy. *ChemCatChem* **2019**, *11*, 3401–3412.
- [13] R. T. Hannagan, G. Giannakakis, R. Réocreux, J. Schumann, J. Finzel, Y. Wang, A. Michaelides, P. Deshlahra, P. Christopher, M. Flytzani-Stephanopoulos, M. Stamatakis, and E. C. H. Sykes, First-principles design of a single-atom–alloy propane dehydrogenation catalyst. *Science* **2021**, *372*, 1444–1447.
- [14] A. Tsiotsias, N. D. Charisiou, I. V. Yentekakis, and M. A. Goula, Bimetallic Ni-based catalysts for CO₂ methanation: a review. *Nanomaterials* **2021**, *11*, 28.

-
- [15] S. Ghosh, S. Hariharan, and A. K. Tiwari, Water adsorption and dissociation on copper/nickel bimetallic surface alloys: effect of surface temperature on reactivity. *J. Phys. Chem. C* **2017**, *121*, 16351–16365.
- [16] H. Yoshida, Y. Kawakami, W. Tokuzumi, Y. Shimokawa, T. Hirakawa, J. Ohyama, and M. Machida, Low-temperature NO reduction over Fe-Ni alloy nanoparticles using synergistic effects of Fe and Ni in a catalytic NO-CO-C₃H₆-O₂ reaction. *Bull. Chem. Soc. Jpn.* **2020**, *93*, 1050–1055.
- [17] L. Zhang, I. A. W. Filot, Y. Su, J. Liu, and E. J. M. Hensen, Transition metal doping of Pd(111) for the NO + CO reaction. *J. Catal.* **2018**, *363*, 154-163.
- [18] H. Hirata, Recent research progress in automotive exhaust gas purification catalyst. *Catal. Surv. Asia* **2014**, *18*, 128–133.
- [19] A. Beniya, Y. Ikuta, N. Isomura, H. Hirata, and Y. Watanabe, Synergistic promotion of NO-CO reaction cycle by gold and nickel elucidated using a well-defined model bimetallic catalyst surface. *ACS Catal.* **2017**, *7*, 1369–1377.
- [20] G. Kyriakou, A. M. Márquez, J. P. Holgado, M. J. Taylor, A. E. H. Wheatley, J. P. Mehta, J. F. Sanz, S. K. Beaumont, and R. M. Lambert, Comprehensive experimental and theoretical study of the CO + NO reaction catalyzed by Au/Ni nanoparticles. *ACS Catal.* **2019**, *9*, 4919–4929.
- [21] F. Besenbacher, I. Chorkendorff, B. S. Clausen, B. Hammer, A. M. Molenbroek, J. K. Nørskov, and I. Stensgaard, Design of a surface alloy catalyst for steam reforming. *Science* **1998**, *279*, 1913–1915.
- [22] A. G. Trant, T. E. Jones, J. Gustafson, T. C. Q. Noakes, P. Bailey, and C. J. Baddeley, Alloy formation in the Au{111}/Ni system – an investigation with scanning tunneling microscopy and medium energy ion scattering. *Surf. Sci.* **2009**, *603*, 571–579.
- [23] P. M. Holmblad, J. H. Larsen, and I. Chorkendorff, Modification of Ni(111) reactivity toward CH₄, CO, and D₂ by two-dimensional alloying. *J. Chem. Phys.* **1996**, *104*, 7289–7295.
- [24] H. Okamoto, *Desk handbook: phase diagrams for binary alloys*, ASM Int. **2000**.
- [25] F. Studt, F. Abild-Pedersen, Q. Wu, A. D. Jensen, B. Temeld, J. D. Grunwaldt, and J. K. Nørskov, CO hydrogenation to methanol on Cu-Ni catalysts: theory and experiment. *J. Catal.* **2012**, *293*, 51–60.
- [26] K. Ray, R. Bhardwaj, B. Singh, and G. Deo, Developing descriptors for CO₂ methanation and CO₂ reforming of CH₄ over Al₂O₃ supported Ni and low-cost Ni based alloy catalysts. *Phys. Chem. Chem. Phys.* **2018**, *20*, 15939–15950.

-
- [27] Y. Yang, Y. A. Lin, X. Y. Yan, F. Chen, Q. Shen, L. M. Zhang, and N. Yan, Cooperative atom motion in Ni-Cu nanoparticles during the structural evolution and the implication in the high-temperature catalyst design. *Acs Appl. Energ. Mater.* **2019**, *2*, 8894–8902.
- [28] D. A. Patel, R. T. Hannagan, P. L. Kress, A. C. Schilling, V. Çınar, and E. C. H. Sykes, Atomic-scale surface structure and CO tolerance of NiCu single-atom alloys. *J. Phys. Chem. C* **2019**, *123*, 28142–28147.
- [29] J. Shan, N. Janvelyan, H. Li, J. Liu, T. M. Egle, J. Ye, M. M. Biener, J. Biener, C. M. Friend, and M. Flytzani-Stephanopoulos, Selective non-oxidative dehydrogenation of ethanol to acetaldehyde and hydrogen on highly dilute NiCu alloys. *Appl. Catal. B: Environ.* **2017**, *205*, 541–550.
- [30] J. Shan, J. Liu, M. Li, S. Lustig, S. Lee, and M. Flytzani-Stephanopoulos, NiCu single atom alloys catalyze the C–H bond activation in the selective non-oxidative ethanol dehydrogenation reaction. *Appl. Catal. B: Environ.* **2018**, *226*, 534–543.
- [31] S. M. Foiles, M. I. Baskes, and M. S. Daw, Embedded-atom-method functions for the fcc metals Cu, Ag, Au, Ni, Pd, Pt, and their alloys. *Phys. Rev. B* **1986**, *33*, 7983–7991.
- [32] H. H. Brongersma, M. J. Sparnaay, and T. M. Buck, Surface segregation in Cu-Ni and Cu-Pt alloys; a comparison of low-energy ion-scattering results with theory. *Surf. Sci.* **1978**, *71*, 657–678.
- [33] S. Kikkawa, K. Teramura, H. Asakura, S. Hosokawa, and T. Tanaka, Ni-Pt alloy nanoparticles with isolated Pt atoms and their cooperative neighboring Ni atoms for selective hydrogenation of CO₂ toward CH₄ evolution: *in situ* and transient Fourier transform infrared studies. *ACS Appl. Nano Mater.* **2020**, *3*, 9633–9644.
- [34] H. Qiu, J. Ran, J. Niu, F. Guo, and Z. Ou, Effect of different doping ratios of Cu on the carbon formation and the elimination on Ni (111) surface: a DFT study. *Mol. Catal.* **2021**, *502*, 111360.
- [35] Y.-F. Wang, K. Li, and G.-C. Wang, Formic acid decomposition on Pt₁/Cu(111) single platinum atom catalyst: insights from DFT calculations and energetic span model analysis. *Appl. Surf. Sci.* **2018**, *436*, 631–638.
- [36] Y. Yang, M. G. White, and P. Liu, Theoretical study of methanol synthesis from CO₂ hydrogenation on metal-doped Cu(111) Surfaces. *J. Phys. Chem. C* **2012**, *116*, 248–256.
- [37] G. Kresse and J. Furthmüller, Efficiency of *ab-initio* total energy calculations for metals and semiconductors using a plane-wave basis set. *Comput. Mater. Sci.* **1996**, *6*, 15–50.

-
- [38] G. Kresse and J. Furthmüller, Efficient iterative schemes for *ab initio* total-energy calculations using a plane-wave basis set. *Phys. Rev. B* **1996**, *54*, 11169–11186.
- [39] J. P. Perdew, K. Burke, and M. Ernzerhof, Generalized gradient approximation made simple. *Phys. Rev. Lett.* **1996**, *77*, 3865–3868.
- [40] P. E. Blochl, Projector augmented-wave method. *Phys. Rev. B* **1994**, *50*, 17953–17979.
- [41] G. Kresse and D. Joubert, From ultrasoft pseudopotentials to the projector augmented-wave method. *Phys. Rev. B* **1999**, *59*, 1758–1775.
- [42] (a) M. P. Teter, M. C. Payne, and D. C. Allan, Solution of Schrödinger's equation for large systems. *Phys. Rev. B Condens Matter.* **1989**, *40*, 12255–12263. (b) D. M. Bylander, L. Kleinman, and S. Lee, Self-consistent calculations of the energy bands and bonding properties of $B_{12}C_3$. *Phys. Rev. B* **1990**, *42*, 1394–1403.
- [43] M. Methfessel and A. T. Paxton, High-precision sampling for Brillouin-zone integration in metals. *Phys. Rev. B* **1989**, *40*, 3616–3621.
- [44] J. Yin, X. Liu, X. -W. Liu, H. Wang, H. Wan, S. Wang, W. Zhang, X. Zhou, B. -T. Teng, Y. Yang, Y. -W. Li, Z. Cao, and X. -D. Wen, Theoretical exploration of intrinsic facet-dependent CH_4 and C_2 formation on Fe_5C_2 particle. *Appl. Catal. B: Environ.* **2020**, *278*, 119308.
- [45] G. Henkelman, A. Arnaldsson, and H. A. Jonsson, fast and robust algorithm for Bader decomposition of charge density. *Comput. Mater.Sci.* **2006**, *36*, 354–360.
- [46] M. J. Frisch, G. W. Trucks, H. B. Schlegel, and G. E. Scuseria, G. E.; *et al.* Gaussian 16, Revision C.01, Gaussian, Inc.: Wallingford, CT, **2019**.
- [47] A. D. Becke, Density-functional exchange-energy approximation with correct asymptotic behavior. *Phys. Rev. A* **1988**, *38*, 3098–3100.
- [48] A. D. Becke, Density-functional thermochemistry. III. The role of exact exchange. *J. Chem. Phys.* **1993**, *98*, 5648–5652.
- [49] C. Lee, W. Yang, and R. G. Parr, Development of the Colle-Salvetti correlation-energy formula into a functional of the electron density. *Phys. Rev. B*, **1988**, *37*, 785–789.
- [50] M. Dolg, U. Wedig, H. Stoll, and H. Preuss, H. Energy-adjusted *ab initio* pseudopotentials for the first row transition elements. *J. Chem. Phys.* **1987**, *86*, 866–872.
- [51] J. M. L. Martin and A. Sundermann, A. Correlation consistent valence basis sets for use with the Stuttgart-Dresden-Bonn relativistic effective core potentials: the atoms Ga-Kr and In-Xe. *J. Chem. Phys.* **2001**, *114*, 3408–3420.
- [52] C. Kittel, *Introduction to Solid State Physics*, 6th ed.; Wiley: **1986**.

-
- [53] D. R. Lide, *CRC Handbook of Chemistry and Physics*, 84th ed.; CRC Press: New York, **2004**.
- [54] A. V. Ruban, H. L. Skriver, and J. K. Nørskov, Surface segregation energies in transition-metal alloys. *Phys. Rev. B* **1999**, *59*, 15990–16000.
- [55] J. Nerlov and I. Chorkendorff, Methanol synthesis from CO₂, CO, and H₂ over Cu(100) and Ni/Cu(100). *J. Catal.* **1999**, *181*, 271–279.
- [56] C. Fan, Y. -A. Zhu, Y. Xu, Y. Zhou, X. -G. Zhou, and D. Chen, Origin of synergistic effect over Ni-based bimetallic surfaces: a density functional theory study. *J. Chem. Phys.* **2012**, *137*, 014703.
- [57] Y. Zhang, X. -R. Shi, C. Sun, S. Huang, Z. Duan, P. Ma, and J. Wang, CO oxidation on Ni-based single-atom alloys surfaces. *Mol. Catal.* **2020**, *495*, 111154.
- [58] B. Hwang, H. Kwon, J. Ko, B. -K. Kim, J. W. Han, Density functional theory study for the enhanced sulfur tolerance of Ni catalysts by surface alloying. *Appl. Surf. Sci.* **2018**, *429*, 87–94.
- [59] We did not consider the cohesive energy because the size of the M_n cluster/particle depends on the experimental conditions and because the cohesive energy depends on the size of the M_n cluster/particle.
- [59] S. Sakaki, B. Biswas, and M. Sugimoto, A Theoretical study of the C–H activation of methane derivatives. Significant effects of electron-withdrawing substituents. *Organometallics*, **1998**, *17*, 1278–1289.
- [60] S. Sakaki, S. Kai, and M. Sugimoto, M. Theoretical Study on σ -Bond Activation of (HO)₂B–XH₃ by M(PH₃)₂ (X = C, Si, Ge, or Sn; M = Pd or Pt). Noteworthy Contribution of the Boryl p_{π} Orbital to M–Boryl Bonding and Activation of the B–X σ -Bond. *Organometallics* **1999**, *18*, 4825–4837.
- [61] B. Biswas, M. Sugimoto, and S. Sakaki, Theoretical study of the structure, bonding nature, and reductive elimination reaction of Pd(XH₃)(η^3 -C₃H₅)(PH₃) (X = C, Si, Ge, Sn). Hypervalent behavior of group 14 elements. *Organometallics*, **1999**, *18*, 4015–4026.
- [62] S. Sakaki, B. Biswas, Y. Musashi, and M. Sugimoto, Bonding nature and reaction behavior of inter-element linkages with transition metal complexes. A theoretical study. *J. Organomet. Chem.*, **2000**, *611*, 288–298.
- [63] M. Ray, Y. Nakao, H. Sato, and S. Sakaki, Theoretical study of tungsten η^3 -silaallyl/ η^3 -vinylsilyl and vinyl silylene complexes: interesting bonding nature and relative stability. *Organometallics*, **2007**, *26*, 4413–4423.

- [64] N. Ochi, Y. Nakao, H. Sato, and S. Sakaki, Theoretical Study of C–H and N–H σ -Bond Activation Reactions by Titanium(IV)-Imido Complex. Good Understanding Based on Orbital Interaction and Theoretical Proposal for N–H σ -Bond Activation of Ammonia. *J. Am. Chem. Soc.* **2007**, *129*, 8615–8624.
- [65] M. Ray, Y. Nakao, H. Sato, H. Sakaba, and S. Sakaki, How to Stabilize η^3 -Silapropargyl/Alkynylsilyl Complex of $[\text{CpL}_2\text{M}]^+$ (L = CO, PMe_3 , or PF_3 and M = W or Mo): Theoretical Prediction. *Organometallics* **2009**, *28*, 65–73.
- [66] S. Sakaki, Theoretical and computational study of a complex system consisting of transition metal element(s): how to understand and predict its geometry, bonding nature, molecular property, and reaction behavior. *Bull. Chem. Soc. Jpn.* **2015**, *88*, 889–938.
- [67] R. L. Zhong and S. Sakaki S. sp^3 C–H borylation catalyzed by iridium(III) triboryl complex: comprehensive theoretical study of reactivity, regioselectivity, and prediction of excellent ligand. *J. Am. Chem. Soc.* **2019**, *141*, 9854–9866.
- [68] J. Lu, B. Zhu, and S. Sakaki, O_2 activation by core-shell $\text{Ru}_{13}@\text{Pt}_{42}$ particles in comparison with Pt_{55} particles: a DFT study. *RSC Adv.* **2020**, *10*, 36090–36100.
- [69] N. Takagi, K. Ishimura, M. Matsui, R. Fukuda, T. Matsui, T. Nakajima, M. Ehara, and S. Sakaki, How can we understand Au_8 cores and entangled ligands of selenolate- and thiolate-protected gold nanoclusters $\text{Au}_{24}(\text{ER})_{20}$ and $\text{Au}_{20}(\text{ER})_{16}$ (E = Se, S; R = Ph, Me)? A theoretical study. *J. Am. Chem. Soc.* **2015**, *137*, 8593–8602.
- [70] J. Lu, K. Ishimura, and S. Sakaki, Theoretical insight into core–shell preference for bimetallic Pt-M (M = Ru, Rh, Os, and Ir) cluster and its electronic structure. *J. Phys. Chem. C* **2018**, *122*, 9081–9090.
- [71] B. Zhu, J. Lu, and S. Sakaki, Catalysis of core-shell nanoparticle $\text{M}@\text{Pt}$ (M = Co and Ni) for oxygen reduction reaction and its electronic structure in comparison to Pt nanoparticle. *J. Catal.* **2021**, *397*, 13–26.
- [72] R. Ferrando, J. Jellinek, and R L. Johnston, Nanoalloys: from theory to applications of alloy clusters and nanoparticles. *Chem. Rev.* **2008**, *108*, 845–910.
- [73] Y. -A. Zhu, D. Chen, X. -G. Zhou, and W. -K. Yuan, DFT studies of dry reforming of methane on Ni catalyst. *Catal. Today*, **2009**, *148*, 260–267.
- [74] J. Carrasco, L. Barrio, P. Liu, J. Rodriguez, and M. V. Ganduglia-Pirovano, Theoretical studies of the adsorption of CO and C on Ni(111) and Ni/CeO₂(111): evidence of a strong metal–support interaction. *J. Phys. Chem. C*, **2013**, *117*, 8241–8250.

-
- [75] X. Guo, H. Liu, B. Wang, Q. Wang, and R. Zhang, Insight into C + O(OH) reaction for carbon elimination on different types of CoNi(111) surfaces: a DFT study. *RSC Adv.*, **2015**, *5*, 19970.
- [76] H. Liu, R. Zhang, F. Ding, R. Yan, B. Wang, and K. Xie, A first-principles study of C + O reaction on NiCo(111) surface. *Appl. Surf. Sci.*, **2011**, *257*, 9455–9460.
- [77] A. Stroppa, K. Termentzidis, J. Paier, G. Kresse, and J. Hafner, CO adsorption on metal surfaces: A hybrid functional study with plane-wave basis set. *Phys. Rev. B*, **2007**, *76*, 195440.
- [78] L. C. Grabow and M. Mavrikakis, Mechanism of methanol synthesis on Cu through CO₂ and CO hydrogenation. *ACS Catal.* **2011**, *1*, 365–384.
- [79] Y. -X. Wang, G. C. Wang, A Systematic theoretical study of water gas shift reaction on Cu(111) and Cu(110): potassium effect. *ACS Catal.* **2019**, *9*, 2261–2274.
- [80] L. Surnev, Z. Xu, and J. T. Yates, IRAS study of the adsorption of CO on Ni(111): Interrelation between various bonding modes of chemisorbed CO. *Surf. Sci.* **1988**, *201*, 1-13.
- [81] K. S. Smirnov and G. Raseev, Coverage dependent IR frequency shift of CO molecules adsorbed on Ni (111) surface. *Surf. Sci.* **1997**, *384*, 875–879.
- [82] B. E. Hayden, K. Kretschmar, and A. M. Bradshaw, An infrared spectroscopic study of CO on Cu(111): The linear, bridging and physisorbed species. *Surf. Sci.* **1985**, *155*, 553-566.